U.S.G.S. Award Number: G12AP20034
Project Dates: 12/02/11 - 12/01/12

Liquefaction Impact on Critical Infrastructure in Christchurch

Jonathan D. Bray[1], Thomas D. O'Rourke[2], Misko Cubrinovski[3], Joshua D. Zupan[1], Sang-Soo Jeon[4], Merrick Taylor[3], Selcuk Toprak[5], Matthew Hughes[3], Sjoerd van Ballegooy[6], and Dimitra Bouziou[2]

[1]University of California, Berkeley, U.S.A.
[2]Cornell University, U.S.A.
[3]University of Canterbury, New Zealand
[4]INJE University, South Korea
[5]Pamukkale University, Turkey
[6]Tonkin and Taylor Ltd., New Zealand

Principal Investigators:

Professor Jonathan D. Bray, Ph.D., P.E.
Department of Civil and Environmental Engineering
University of California, Berkeley
Berkeley, CA 94720-1710
Tel. (510) 642-9843; Fax. (510) 642-7476
bray@ce.berkeley.edu
URL: http://www.ce.berkeley.edu/~bray/

Professor Thomas O'Rourke, Ph.D.
School of Civil and Environmental Engineering
Cornell University
Ithaca, NY 14583
Tel: 607-255-6470; Fax: 607-255-9004
tdo1@cornell.edu
URL: http://www.cee.cornell.edu/cee/people/profile.cfm?netid=tdo1

Final Technical Report

March 22, 2013

U.S.G.S. Award Number: G12AP20034

Liquefaction Impact on Critical Infrastructure in Christchurch

Jonathan D. Bray, Univ. of California, Berkeley, Thomas D. O'Rourke, Cornell Univ., Misko Cubrinovski, Univ. of Canterbury, Joshua D. Zupan, Univ. of California, Berkeley, Sang-Soo Jeon, INJE Univ., Merrick Taylor, Univ. of Canterbury, Selcuk Toprak, Pamukkale Univ., Matthew Hughes, Univ. of Canterbury, Sjoerd van Ballegooy, Tonkin & Taylor, and Dimitra Bouziou, Cornell Univ.

ABSTRACT

The Canterbury earthquake sequence provides an exceptional opportunity to investigate the effects of varying degrees of liquefaction on the built environment, including buildings and lifelines. Liquefaction during the earthquake sequence damaged medium and low rise reinforced concrete and steel buildings, masonry buildings, industrial facilities, and timber-frame residential structures, as well as lifelines, including water supply, wastewater, drainage, natural gas, electric power, telecommunications, and transportation networks. Ground deformation varied from strong shaking in the absence of permanent soil displacement to large levels of liquefaction-induced lateral spreading and settlement. Research on these earthquakes provides an unprecedented opportunity to develop an integrated understanding of how critical infrastructure performs in a major earthquake with extensive and damaging liquefaction. Rarely has detailed information about lifeline and building performance been available to the degree that exists for Christchurch where the liquefaction effects of several earthquakes can be documented in a comprehensive way for both buildings and lifelines.

Many multi-story buildings in the Central Business District were heavily damaged by liquefaction-induced ground movements during the 22 February 2011 M_w 6.2 Christchurch earthquake, but not other earthquakes. CPT-based liquefaction triggering evaluations were conservative. The conservatism in the liquefaction triggering assessments led to post-liquefaction ground settlement estimates that were generally similar for the large events in the earthquake sequence, whereas significant ground settlements and building damage in the CBD were only observed for the Christchurch earthquake. Moreover, the liquefaction-induced ground settlement procedures do not capture important shear-induced deformation mechanisms and the effects of ground loss due to sediment ejecta. Performance-based earthquake engineering requires improved procedures to predict the differing levels of performance observed in Christchurch.

Additionally, key aspects of underground lifeline system performance, using data acquired for the Canterbury earthquake sequence, was explored. The seismic performance of the water supply, wastewater, and natural gas distribution systems to the 4 September 2010 M_w 7.1, 22 February 2011 M_w 6.2, and 13 June 2011 M_w 6.0 earthquakes were studied in great detail. Repair rates, expressed as repairs/km, for different types of pipelines are evaluated relative to the spatial distribution of peak ground velocity outside liquefaction areas, and differential ground surface settlement and lateral ground strain within areas affected by liquefaction, which was calculated from high resolution LiDAR survey data acquired before and after each main seismic event. The excellent performance of the gas distribution network is the result of highly ductile polyethylene pipelines. Lessons learned regarding the earthquake performance of underground lifeline systems are summarized.

Table of Contents

1. INTRODUCTION

The 22 February 2011 Christchurch M_w 6.2 earthquake caused 185 fatalities and left many others seriously injured. Most of the damage was within the Central Business District (CBD) of Christchurch. Seventy percent of the nearly 3,000 buildings within the CBD prior to the earthquake have been or will be demolished due to earthquake damage. The seismic performance of modern commercial and residential buildings and their supporting buried utilities in the CBD were often significantly impacted by soil liquefaction.

The data collected for the Canterbury earthquake sequence, which also included the 4 September 2010 Darfield M_w 7.1 and 13 June 2011 M_w 6.0 earthquakes, are unprecedented in size and detail, involving ground motion recordings from scores of seismograph stations, high resolution light detection and ranging (LiDAR) surveys of the ground surface before and after each main seismic event allowing vertical and lateral ground surface movements to be calculated, detailed repair records for thousands of km of underground pipelines, and in-depth surveys of damage to structures that are well documented with building plans and pre-earthquake site investigations.

The Canterbury earthquake sequence provides an exceptional opportunity to investigate the effects of varying degrees of liquefaction on the built environment, including buildings and lifelines. Liquefaction during the earthquake sequence damaged medium and low rise reinforced concrete and steel buildings, masonry buildings, industrial facilities, and timber-frame residential structures, as well as lifelines, including water supply, wastewater, drainage, natural gas, electric power, telecommunications, and transportation networks. Ground deformation varied from strong shaking in the absence of permanent soil displacement to large levels of liquefaction-induced lateral spreading and settlement.

In this report, the results of parallel studies of the seismic performance of structures located in the CBD (Section 2) and the seismic performance of water supply, wastewater, and natural gas distribution systems across the wider Christchurch region (Section 3) are presented. Research on the effects of the Canterbury earthquake sequence provides an unprecedented opportunity to develop an integrated understanding of how critical infrastructure performs in a major earthquake with extensive and damaging liquefaction. Rarely has detailed information about lifeline and building performance been available to the degree that exists for Christchurch where the liquefaction effects of several earthquakes can be documented in a comprehensive way for both buildings and lifelines. It is hoped that these investigations will provide the underlying data and understanding for advancing an integrated examination of the impacts of liquefaction on critical infrastructure in the United States.

2. LIQUEFACTION EFFECTS ON BUILDINGS IN THE CENTRAL BUSINESS DISTRICT OF CHRISTCHURCH

2.1 Introduction

The 22 February 2011 Christchurch M_w 6.2 earthquake caused 185 fatalities and left many others seriously injured. Most of the damage was within the Central Business District (CBD) of Christchurch. Seventy percent of the nearly 3,000 buildings within the CBD prior to the earthquake have been or will be demolished due to earthquake damage. The seismic performance of modern commercial and residential buildings and their supporting buried utilities in the CBD were often significantly impacted by soil liquefaction. This section presents the results of a comprehensive site characterization program that employed primarily the cone penetration test (CPT) to evaluate liquefaction triggering and its effects on buildings in the CBD.

Following the Christchurch earthquake, Tonkin & Taylor (T&T) was commissioned to characterize generally the subsurface conditions within the CBD. This characterization effort included 48 boreholes, 151 CPTs, 45 km of geophysical surveys, installation of piezometers, and laboratory testing of collected soil samples. The UC Berkeley (UCB)-Univ. of Canterbury (UC) research team performed an additional 71 CPTs and 2 boreholes within 6 zones that encompassed 23 structures to enable detailed subsurface characterizations and simplified seismic evaluations of representative buildings within the CBD. These structures consisted of multi-story buildings on shallow and deep foundations and displayed interesting engineering performance characteristics. This subset included buildings that performed well, in addition to buildings that were severely damaged during the Christchurch earthquake. In this section, the investigation and evaluation of several of the most insightful building case histories are presented.

2.2 2010-11 Canterbury Earthquakes Shaking

The Canterbury earthquake sequence included seven events with $M_w \geq 5.5$, three of which had $M_w \geq 6.0$. Ground shaking was recorded at four strong motion stations (SMS) within the CBD, the locations of which are shown in Fig. 2.1. The geometric mean horizontal peak ground accelerations (*PGA*) recorded at the stations are provided in Table 2.1 for ten events. The 22 FEB 11 Christchurch M_w 6.2 earthquake produced the most intense ground shaking in the CBD, because the source-to-site distances (R) were only 3-6 km. Its *PGA* values were twice those recorded during the larger, but more distant (R = 18-20 km), 4 SEP 10 Darfield M_w 7.1 event. The *PGA*s recorded in the CBD during the Darfield event are similar to those recorded during the 26 DEC 10 M_w 4.8, 13 JUN 11 M_w 6.0, and 23 DEC 11 M_w 5.9 events. The *PGA* values of the dozens of other M_w 5^+ events are lower than those recorded during these events. The Canterbury earthquake sequence provides an unparalleled opportunity to investigate the effects of varying degrees of liquefaction on the built environment.

Table 2.1. Recorded *PGA*s in the CBD during the 2010-11 Canterbury earthquake sequence

Date	M_w	Geometric Mean *PGA* (g) at CBD Recording Stations				Median *PGA* (g)
		CBGS	CCCC	CHHC	REHS	
4 SEP 10	7.1	0.17	0.21	0.18	0.25	0.20
26 DEC 10	4.8	0.25	0.22	0.16	0.24	0.23
22 FEB 11	6.2	0.48	0.42	0.35	0.51	0.45
22 FEB 11	5.5	-	0.14	0.17	-	0.16
22 FEB 11	5.6	-	0.09	0.09	-	0.09
16 APR 11	5.0	0.07	-	0.15	0.10	0.10
13 JUN 11	5.3	0.18	-	0.20	0.18	0.18
13 JUN 11	6.0	0.16	-	0.21	0.29	0.21
23 DEC 11	5.8	0.16	0.14	0.18	0.21	0.17
23 DEC 11	5.9	0.20	0.18	0.21	0.30	0.21

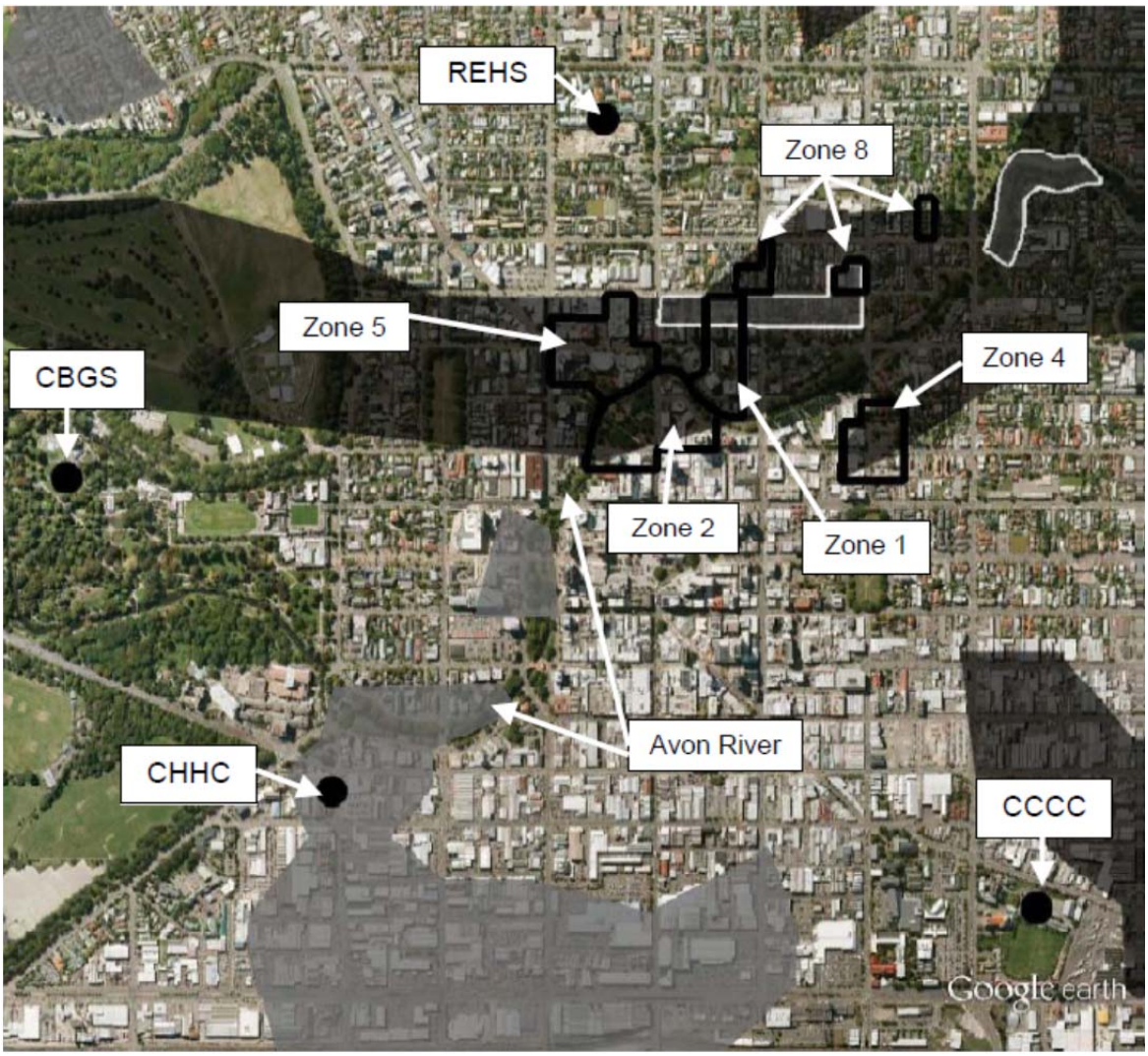

Figure 2.1. CBD location plan with strong ground motion recording stations and study zones. Shaded zones indicate areas with surficial evidence of soil liquefaction: dark shading indicates moderate to severe liquefaction and gray shading indicates low to moderate liquefaction during the 22 FEB 11 event; white outlining indicates areas that also liquefied during the 4 SEP 10 and 13 JUN 11 events

The Christchurch earthquake produced the most liquefaction in the CBD. The Darfield and June 2011 earthquakes also produced liquefaction. Hence, these events are explored in more depth. However, examining the less damaging events is also important, because it is critical to evaluate if liquefaction evaluation procedures can discern between damaging events and non-damaging events. The 26 DEC 10 event is useful for this purpose, as no liquefaction was observed in the CBD for this event. The acceleration-time histories recorded at the REHS station for these four events are shown in Fig. 2.2a. The differing intensities and durations of these events are readily apparent. The characteristics of the ground motions recorded in the CBD are described further through 5% damped elastic acceleration response spectra and Arias intensity-time histories in Figs. 2.2b and 2.2c. The intensity and shaking intensity rate (*SIR*) of the ground motions of the Christchurch event indicate why it was most damaging. The parameter *SIR* captures the amount of increase of the Arias Intensity over the period of strongest shaking (Bray and Dashti 2010), and it is highest for the Christchurch earthquake. The distinguishing feature of the Darfield event relative to the other earthquakes is its longer significant duration ($D_{5\text{-}95}$) of 30 s or so. The complexities of the seismic demand are reduced down to the two parameters of *PGA* and M_w in state-of-the-art liquefaction triggering analyses. The details of ground motion shaking displayed in Fig. 2.2 are useful for interpreting the results of the liquefaction evaluation procedures discussed later in the section.

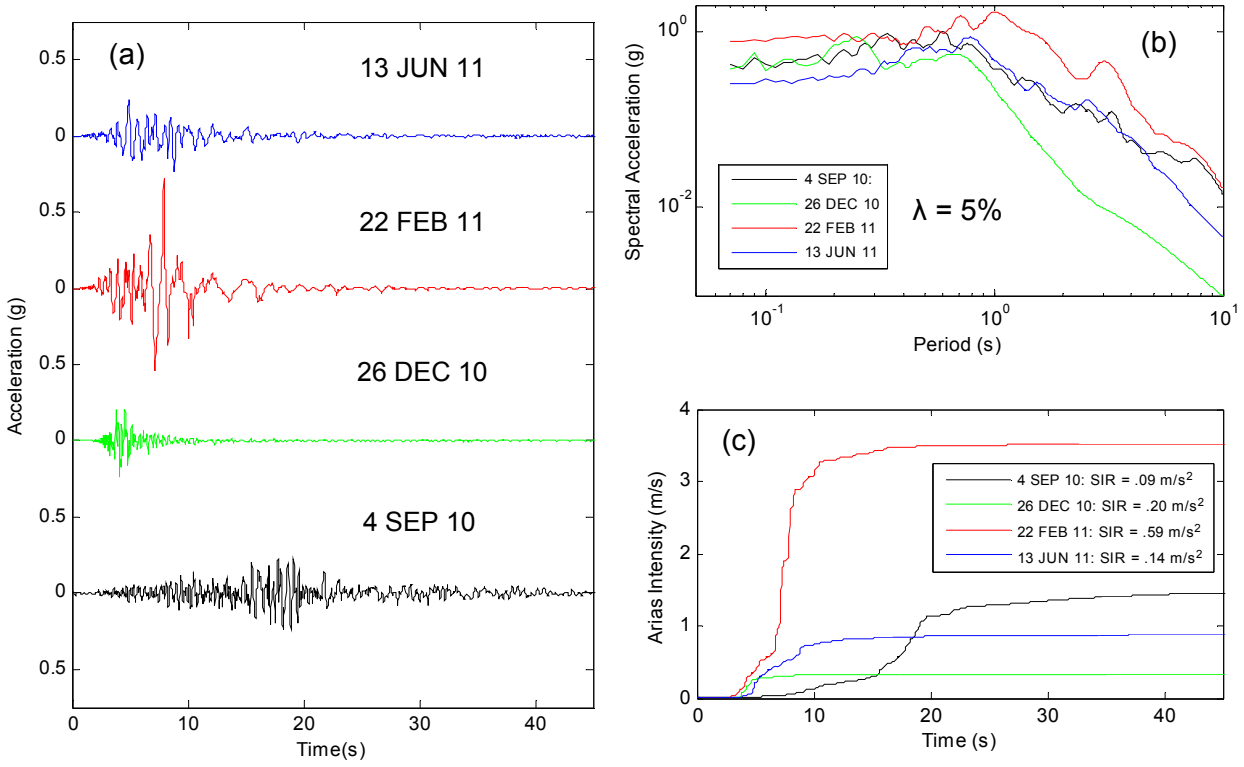

Figure 2.2. (a) Recorded acceleration histories, (b) 5% damped pseudo-acceleration response spectra, and (c) Arias intensity histories at REHS SMS at azimuth 092.

2.3 Overview of Damage Within the CBD

The UC and Geotechnical Extreme Events Reconnaissance (GEER) researchers performed post-earthquake reconnaissance in the CBD after significant events during the 2010-11 Canterbury earthquake sequence. Engineers from T&T also documented damage. Some of these observations have been documented in Green and Cubrinovski (2010) and Cubrinovski et al. (2011a,b,c). Liquefaction severity maps were developed by UC researchers based on observations of sediment ejecta, lateral spreading, and structural settlement following the Darfield, Christchurch, June 2011, and December 2011 events. In addition, a tremendous amount of data, aerial photographs, groundwater models, interpretive maps, investigation reports, and technical guidance, much of which was developed by T&T, are provided through the Canterbury Geotechnical Database (CGD 2012).

Liquefaction in parts of the CBD along the Avon River was severe during the Christchurch earthquake. The shaded zones in Fig. 2.1 delineate the areas with surficial evidence of moderate-to-severe (dark shading) and low-to-moderate (light shading) liquefaction in the Christchurch earthquake. The east-west trending band of moderate-to-severe liquefaction that follows much of the Avon River through the middle of the northern half of the CBD is particularly interesting, because there were many buildings with different foundation types located within this band. Liquefaction was often the controlling factor in terms of structural damage in the band of moderate-to-severe liquefaction. Accordingly, five of the six building zones that were investigated are located in or near this band. The sixth zone, which is not shown in Fig. 2.1, is located southeast of the CCCC SMS in an area of deep liquefiable sands that affected the seismic performance of two buildings that were nearly identical except for one being about twice the plan area as the other.

Cubrinovski et al. (2011a) discusses in detail observations of liquefaction and its effects on structures located in the CBD during the Christchurch earthquake. Buildings shifted laterally toward the banks of the Avon River, they underwent liquefaction-induced tilt or punching failure, or their structural frames were distorted due to liquefaction-induced differential movements of their foundations. Most of the affected buildings were supported on shallow foundations (i.e., reinforced concrete (RC) spread footings connected by tie beams or mats), but several buildings were supported on piles. The liquefaction-induced damage in the CBD is remarkable due to it pervasiveness in the bands shown in Fig. 2.1.

In contrast to the heavy liquefaction-induced damage to buildings in the CBD during the Christchurch earthquake, the Darfield, June 2011, and December 2011 events produced minor to no liquefaction in the CBD. While liquefaction effects in the CBD during these events were insignificant relative to liquefaction during the Christchurch earthquake as well as liquefaction outside of the CBD during these events, it is crucial to note that liquefaction did occur in the CBD during these three events. Although liquefaction occurred at some of the CBD sites during the Darfield, June 2011, and December 2011 events, its effects on buildings and lifelines were minor. No liquefaction occurred in the CBD during the December 2010 earthquake.

2.4 Simplified Liquefaction Evaluation Procedures

Three CPT empirical liquefaction evaluation procedures were used to calculate the factor of safety against liquefaction triggering (FS_l): Robertson and Wride (1998), henceforth called RW98; Moss, Seed et al. (2006), henceforth MS06; and Idriss and Boulanger (2008), henceforth IB08. The seismic demand is characterized using the cyclic stress ratio (*CSR*) for an equivalent $M_w = 7.5$ event as:

$$CSR_{7.5} = 0.65 \frac{PGA}{g} \frac{\sigma_v}{\sigma_v'} r_d \frac{1}{MSF} \quad (2.1)$$

where *PGA* is the horizontal peak ground acceleration at the ground surface, expressed in terms of the acceleration of gravity (g), σ_v and σ_v' are respectively the total and effective vertical stress at the depth of interest, r_d is a depth reduction factor that accounts for soil response during shaking, and *MSF* is a magnitude (i.e., duration) scaling factor used to normalize the *CSR* to that of an equivalent M_w 7.5 earthquake. While each procedure utilizes an empirical approach wherein the estimated $CSR_{7.5}$ for each site is plotted versus a confining stress normalized CPT tip resistance and denoted as either liquefaction was observed or not observed, each correlation was developed uniquely, so that it is essential that each procedure be implemented using the developers' recommended parameters. Differences should be expected and can be considered part of the epistemic uncertainty in liquefaction triggering evaluation.

To capture the aleatory uncertainty in earthquake ground shaking at individual building sites within the CBD, the Bradley and Hughes (2012) study is employed to estimate the median, 16%, and 84% values of *PGA* for the Darfield, Christchurch, and June 2011 events, as shown in Table 2.2. They accounted for the spatial variation in ground motion by conditioning the ground motion prediction equation developed by Bradley (2010) on the recorded *PGA*s at the SMS during each event. The median *PGA* values estimated in the CBD by Bradley and Hughes (2012) are similar to the median of the recorded *PGA*s for these three events. However, their study provides a more robust estimate of the expected range of *PGA* at sites within the CBD. At shallow depths just below the groundwater, it is reasonable to assume r_d and the ratio of vertical effective stress to vertical total stress are nearly one. Assuming the *MSF* recommended in IB08, these *PGA* values can be used to estimate $CSR_{7.5}$ for evaluating shallow liquefaction triggering as noted in Table 2.2. The seismic demand for liquefaction triggering (i.e., $CSR_{7.5}$) during the Christchurch earthquake was about 60% greater than that of the Darfield earthquake, about 90% greater than that of the June 2011 event, and 160% greater than that of the December 2010 event.

Table 2.2. Shallow cyclic stress ratios in the CBD during primary 2010-11 Canterbury earthquakes (*PGA* from Bradley and Hughes, 2012; except for 26 DEC 10)

Event	M_w	PGA_{16}	PGA_{50}	PGA_{84}	$MSF^{\dagger}$	$CSR_{7.5}{}^{*}$
22 FEB 11	6.2	0.34	0.45	0.60	1.41	0.16 - 0.28
4 SEP 10	7.1	0.17	0.22	0.29	1.11	0.10 - 0.17
13 JUN 11	6.0	0.18	0.25	0.35	1.48	0.08 - 0.15
26 DEC 10	4.8	-	0.21	-	1.80	0.08

* $CSR_{7.5} = 0.65(PGA/g)/MSF$ at shallow depth

† $MSF = 6.9 \exp(-M_w/4) - 0.058 \leq 1.8$

If liquefaction triggering is likely, post-liquefaction residual shear strength (S_{ur}) correlations (e.g., Olson & Stark, 2002; IB08) can be utilized to estimate S_{ur}, so that the pseudostatic *FS* against bearing failure could be calculated as a check of seismic stability. The Zhang et al. (2002), henceforth ZR02, procedure can be applied to estimate free-field, level ground, surface settlements due to post-liquefaction volumetric strains. This procedure was developed based on the results of laboratory testing on clean sand presented by Ishihara and Yoshimine (1992). The ZR02 procedure is also used in practice for silty soils. The clean sand equivalent, normalized, CPT tip resistance $q_{c1N\text{-}CS}$ as well as the FS_l were calculated in accordance with the RW98 and IB08 correlations in this study. Consequently, these procedures are henceforth referred to as ZR02-RW98 and ZR02-IB08, respectively.

Although these procedures were developed to estimate vertical settlements at level ground free-field sites due to post-liquefaction volumetric strains, they are often employed in engineering practice to get a sense of the seismic performance of the soils beneath buildings. However, other settlement mechanisms exist for the case of shallow-founded buildings sited atop shallow liquefiable soils, such as SSI-induced ratcheting, partial bearing failure, and ground loss due to sediment ejecta (e.g., Bray and Dashti 2010). Shear-induced mechanisms can contribute significantly to the observed building settlement when soils beneath its foundation elements soften due to liquefaction. However, established simplified methods for estimating shear-induced building settlements are not available currently. Thus, the post-liquefaction reconsolidation settlement calculations are performed to assess the validity of the insights gained from performing these analyses. Currently employed liquefaction-induced building movement evaluation procedures need to be revised to capture these other mechanisms.

2.5 Generalized Subsurface Conditions in the CBD

The Canterbury Plains are composed of complex alluvial fans deposited by eastward-flowing rivers draining the Southern Alps and discharging into Pegasus Bay on the Pacific Coast. Christchurch lies along the eastern extent of the Canterbury Plains, just north of the Banks Peninsula, the eroded remnant of the extinct Lyttelton Volcano, comprised of weathered basalt and Pleistocene loess (Cubrinovski et al. 2011a). The city was built on a historic floodplain of the Waimakiriri River, a large braided river that is now channelized approximately 25 km north of the CBD. The Waimakiriri River regularly flooded Christchurch prior to the construction of levees and river realignment carried out shortly after the city was established in the 1850s (Brown and Weeber 1992; Brown et al. 1995). The "Black" Maps depict several buried stream channels through the CBD, which intersect the study zones (Cubrinovski et al. 2011a). The subsurface conditions in the CBD are highly variable with alternating layers of sands and gravels with overbank deposits of silty soils and some peat pockets, which is indicative of the ephemeral nature of floodplains.

There are three geological formations of primary interest in foundation engineering within the CBD: the Springston Formation, Christchurch Formation, and Riccarton Gravels. The Springston Formation was deposited during the last 3000 years and is the shallowest of the three formations. It consists of three lithologic units (Brown and Weeber 1992): 1) gravels deposited in old flood channels of the Waimakariri River; 2) overbank alluvial silt and sandy silt; and 3) peat deposits formed in marshland. The Christchurch Formation consists of beach, estuarine, lagoon, dune, and coastal swamp deposits composed of gravel, sand, silt, clay, shells, and peat, and its top is found at a depth of typically 7 to 10 m. Brown and Weeber (1992) describe its age

as post-glacial and likely less than 6,500 years old near the maximum inland extent of the post-glacial marine transgression, which likely extended across the CBD based on the presence of shells observed in soil samples (T&T 2011). The Riccarton Gravels are beneath the Christchurch formation and consist of well-graded brown or blue-gray gravels up to cobble size. This 10 to 20 m thick formation is the uppermost confined gravel aquifer in coastal northern Canterbury and is typically about 18 to 30 m below the ground surface in the CBD (Brown and Weeber 1992; T&T 2011).

Two spring fed rivers, the Avon and Heathcote, meander through Christchurch and discharge into an estuary east of Christchurch. The Avon River, labeled in Fig. 2.1, meanders through the CBD, while the Heathcote River flows south of the CBD. Much of the observed moderate-to-severe liquefaction within and to the east of the CBD occurred near the Avon River during the Canterbury earthquakes. The groundwater table is generally within 1 to 3 meters of the ground surface within the CBD.

2.6 Site Investigations

A collaborative study by UC, UCB, Cornell Univ., and Virginia Tech documented and investigated liquefaction-induced damage from the Canterbury earthquakes. As part of this study, the UCB-UC research team performed 71 CPTs (as per ASTM D5778-07) and 2 boreholes in the six building study zones. A standard CPT was advanced after sufficient data had been collected with a CPT with pore water pressure measurements (CPTu), because penetration was often difficult due to gravel layers and porewater pressure corrections were negligible. The 10 cm^2 electrical cones were manufactured by A.P. van den Berg (Icone ELCI-10) with the CPTu filter element located in the standard position just above the base of the cone. It consisted of greased stainless steel and was saturated with silicone oil.

Though subsurface conditions within the CBD are variable (Brown and Weeber 1992; T&T 2011), each building study zone has one or two representative soil profiles that reflect the subsurface conditions within a zone. Figure 2.3 illustrates representative subsurface conditions within Zone 1 with the log of Borehole K1 and the adjacent CPTZ1-B4 with its normalized cone tip resistance (q_{c1N}) and soil behavior type index (I_c) profiles calculated using RW98. The soil layer that lies within the depths of about 2 to 8 m has relatively low q_{c1N} values (< 50) and consists of predominantly silty sand (SM), but also sandy silt (ML), with a median fines content (FC) of approximately 37% (range of 15% to 82% with a standard deviation of 21%) based on 19 laboratory tests performed on retrieved samples. The fines were predominantly nonplastic. Below it, a denser poorly graded sand (SP) extends down to about 20 m. The base silt/clay (ML/MH) layer is the oldest and deepest material of the Christchurch Formation and is typically observed just above the Riccarton Gravels (T&T 2011).

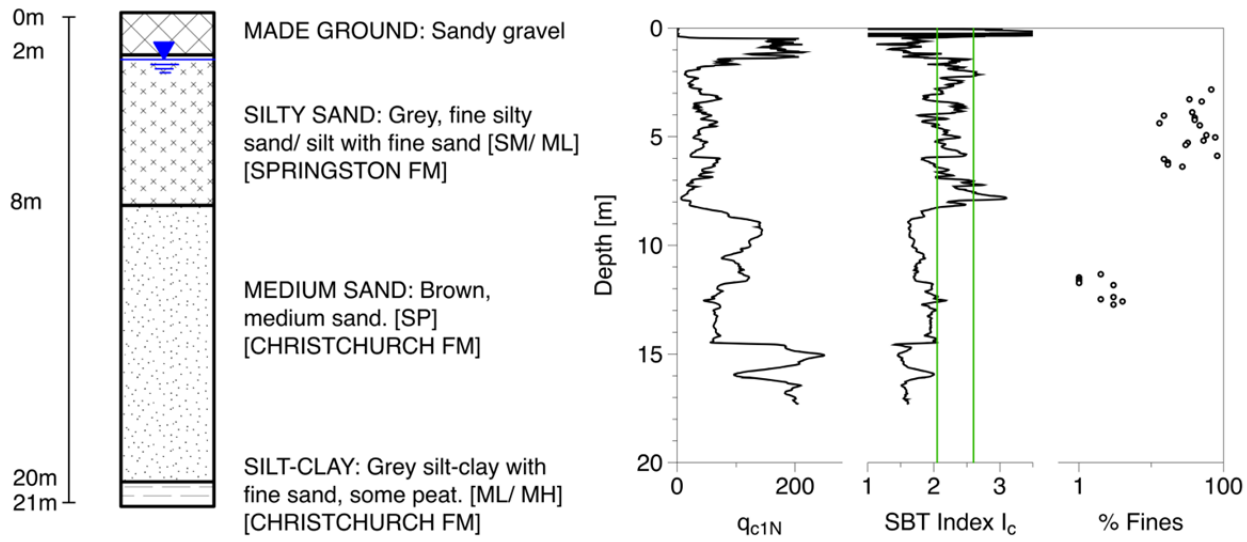

Figure 2.3. Log of borehole K1 and adjacent CPTZ1-B4 profile in Zone 1.

In addition to advancing CPTs adjacent to buildings, a line of 13 CPTs spaced about 10 m apart were advanced in a parking lot at the northeast corner of the intersection of Armagh and Madras streets (S43.5284 E172.6432) to characterize the variability in soil conditions over relatively short distances. At this location within Zone 4, along the southern boundary of the moderate-to-severe liquefaction zone illustrated in Fig. 2.1, Cubrinovski et al. (2011a) observed that liquefaction was manifested by a "*well-defined, narrow zone of surface cracks, fissures, and depression of the ground surface about 50 m wide, as well as water and sand ejecta*." A cross section that depicts the cone tip resistance profiles on the north end of the line is shown in Fig. 2.4. The shallowest layer is composed of silty sand and sandy silt (SM/ ML) with a q_t generally less than 5MPa and I_c between 2.0 and 2.5. Samples from a nearby borehole indicated a FC of about 50% for this layer. The next layer was a clean sand to gravelly sand (SP) with q_t greater than 20 MPa and often greater than 30 MPa and I_c between 1.0 and 1.5. Clean to silty sands of varying penetration resistance, but typically with q_t greater than 10 MPa followed the dense SP layer. The portion of the shallowest layer that was below the groundwater table should have liquefied based on the median *PGA* during the Christchurch earthquake using the RW98 liquefaction triggering procedure. The resulting post-liquefaction vertical settlement using the ZR02 procedure within this layer decreased from a local maximum of about 10 cm in the middle of the liquefaction feature to zero over a total width of 45 m, which is consistent with the dimensions of the surficial depression in this area documented by Cubrinovski et al. (2011a). Consequently, the shallow liquefiable SM/ML layer, when it existed, was likely a critical layer in the observed liquefaction in Zone 4, and in other zones with similar stratigraphy. Its thickness below the water table could vary considerably over relatively short distances.

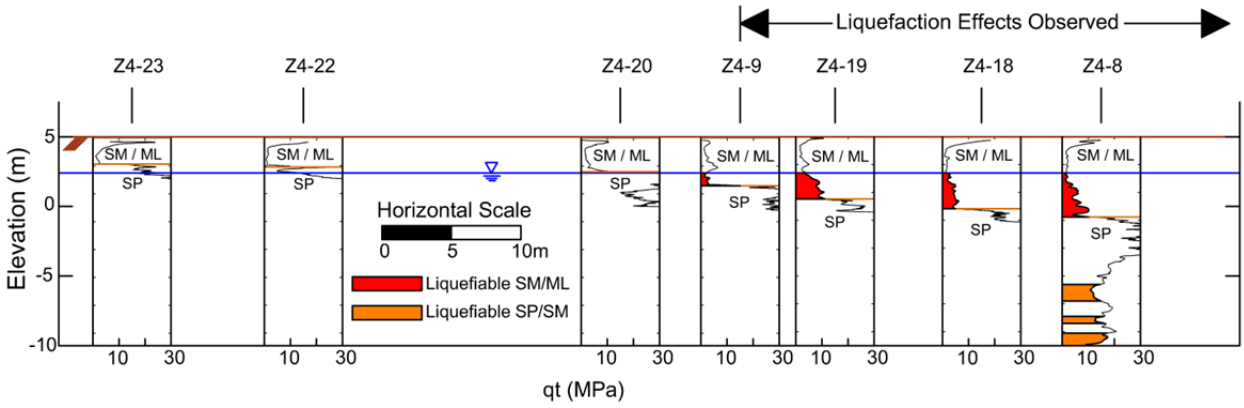

Figure 2.4. Corrected CPT tip resistance profiles showing variability in the thickness of the shallow SM/ML layer across the Armagh and Madras parking lot.

2.7 CBD Buildings Affected by Liquefaction

2.7.1 CTUC Building in Zone 4

The CTUC Building (S43.5286 E172.6425) is located only 20 m west of the Armagh-Madras parking lot discussed previously. It was a 6-story RC frame structure with RC core walls and block in-fill walls with its roof supported by steel framing (Fig. 2.5a). Based on its 1974 design drawings, the building frame was largely supported on shallow footings interconnected with tie beams (Fig. 2.6). Six square footings were 2.44 by 2.44 m and were either 0.46 m or 0.61 m deep, and the two footings at the south end were 4.88 m by 0.91 m and 0.46 m deep. Each of these footings supported a single, rectangular RC column. The center-to-center spacing of the columns in the N-S direction was approximately 4.9 m. A larger footing on the west side of the building supported two rectangular RC columns in addition to the walls associated with the elevator and stair core, and strip footings supported core walls at the SW corner of the building and a block wall on its northern end. Adjacent footings were connected with RC tie beams that had cross sectional areas of either 0.74 m^2 or 0.12 m^2. Floors two through six were RC and were supported by RC beams 0.41 m wide by 0.61 m deep. Footing contact pressures for the effective seismic building weight were 100-200 kPa.

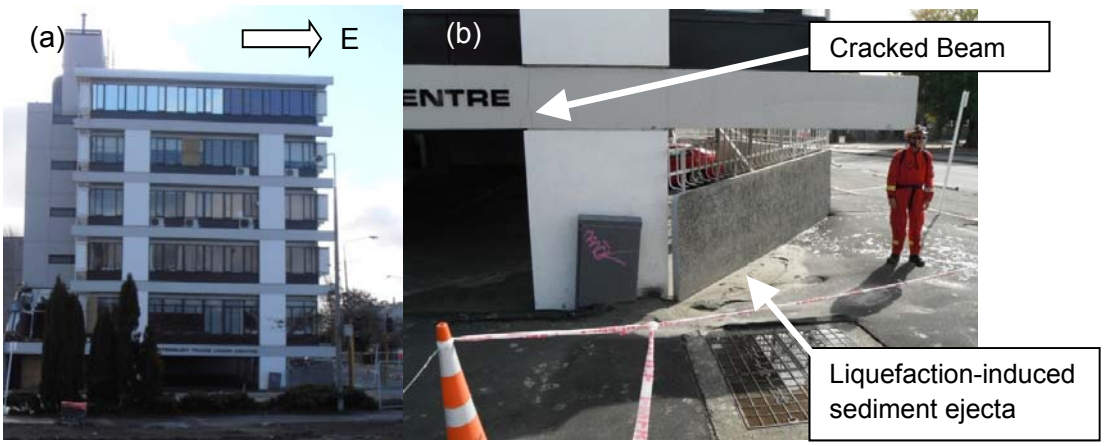

Figure 2.5. (a) South end of CTUC Building showing tilt to the east (taken July 2011) and (b) Close-up photograph of the SE corner of the building (taken March 2011).

While damage to the building was negligible during the Darfield and June 2011 events, severe liquefaction of the foundation soils during the Christchurch earthquake induced significant total and differential settlements of the building, leading to structural distortions and cracking (Cubrinovski et al. 2011a). The building tilted to the east 0.4-0.5 degrees. Differential settlement of the SE corner of the building produced most of the structural damage. Several of the exposed beams on the south side of the building were cracked near the beam-column connections (Fig. 2.5b). Building settlement measurements were performed using the building located just to the north of CTUC Building as the datum, as it did not displace relative to the surrounding ground. The settlement measurements are presented in Fig. 2.6. The building settled more on its south side than on its north side and more on its east side than its west side. Approximately 20 cm of the 25 cm of differential building settlement along the eastern side of the building was measured over the combined length of the two southernmost spans (angular distortion ≈ 1/50). Thus, cracking of structural beams in this area is not surprising.

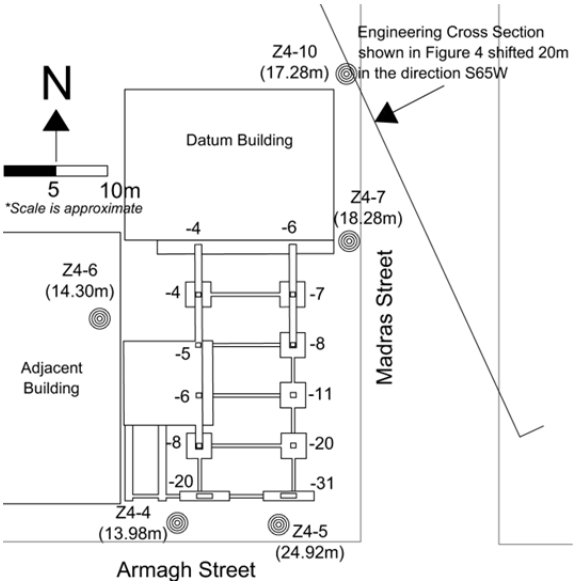

Figure 2.6. CTUC Building site with its foundation system and CPT locations (with depths). Footing settlements at column locations relative to the datum building are provided in cm.

Five CPTs were performed at the site. The generalized subsurface conditions along the east side of the building are depicted in Fig. 2.7. The groundwater depth was estimated to be 2.5 m for the Darfield, December 2010, and Christchurch earthquakes, and 2.0 m for the June 2011 earthquake based on the T&T (2012) groundwater model. The shallow SM/ML layer is similar to the upper unit described previously in Fig. 2.4 and had $q_t < 3$ MPa, $2 < I_c < 2.5$, and nonplastic FC $\approx 50\%$, which makes it likely to liquefy under strong ground shaking. It is noteworthy that this unit was observed at CPT Z4-5, which is at the SE corner of the building, to a depth of nearly 6 m; whereas it was not observed at CPT Z4-7 at the NE corner of the building or below the groundwater table at CPT Z4-10.

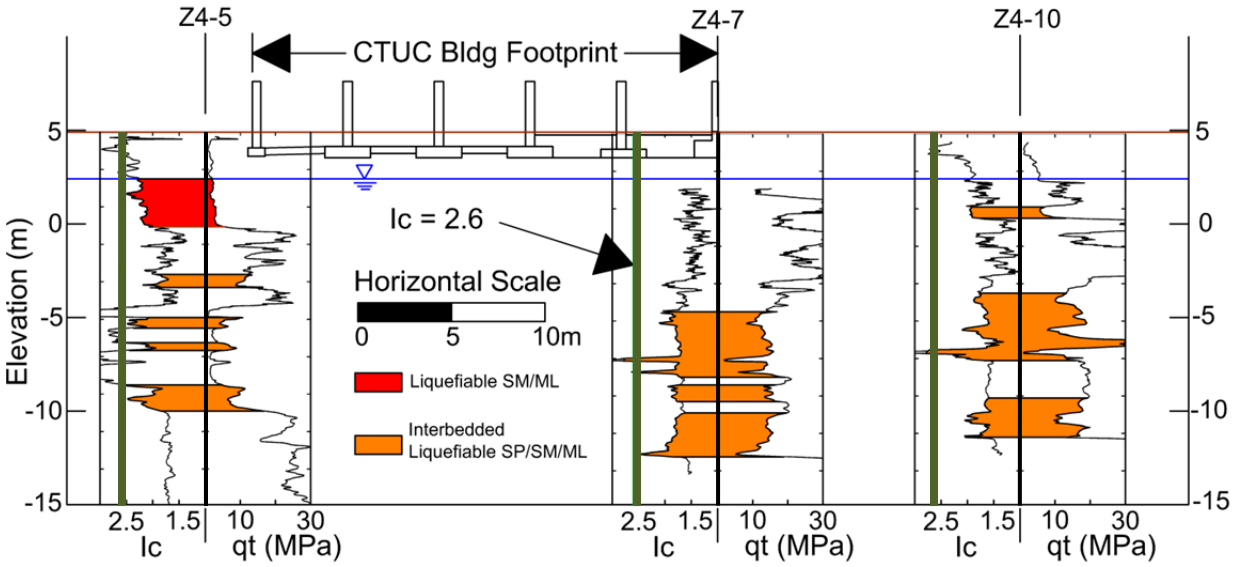

Figure 2.7. Subsurface conditions at CTUC site showing zones of materials with $FS_l < 1.0$ based on the RW98 procedure using PGA_{50} from Bradley and Hughes (2012) for the Christchurch earthquake.

Simplified liquefaction evaluations were performed utilizing the procedures described previously. From examining Fig. 2.7, it is clear that while there are liquefiable soils at each of the CPT locations, the distinguishing difference between them is that CPT Z4-5 indicates that there are shallow liquefiable soils just beneath the building foundation whereas the liquefiable soils at CPTs Z4-7 and Z4-10 are located primarily at depths below 8 m. The dramatic change in the shallow soil conditions from the building's north end, which did not contain shallow liquefiable soils, to its south end, which contained shallow liquefiable soils, led to significant differential settlement over the southernmost spans of the building frame.

The calculated FS_l profiles for four events at CPT Z4-5 are presented in Fig. 2.8 for the median *PGA* estimates. As discussed previously, low FS_l values were calculated in the shallow SM/ML layer for the intense Christchurch earthquake, wherein severe liquefaction was observed at the site. However, FS_l values below one are also calculated for the Darfield and June 2011 earthquakes. Although there were no reports of liquefaction at this location after these events, it is possible that a minor amount of liquefaction was unreported or that marginal liquefaction occurred and surface manifestations were not observed. Damage was not reported for these events, so if liquefaction did occur its effects were insignificant. Liquefaction triggering procedures are deliberately conservative, so it is also possible that liquefaction did not occur at this site although the calculated FS_l values were below one.

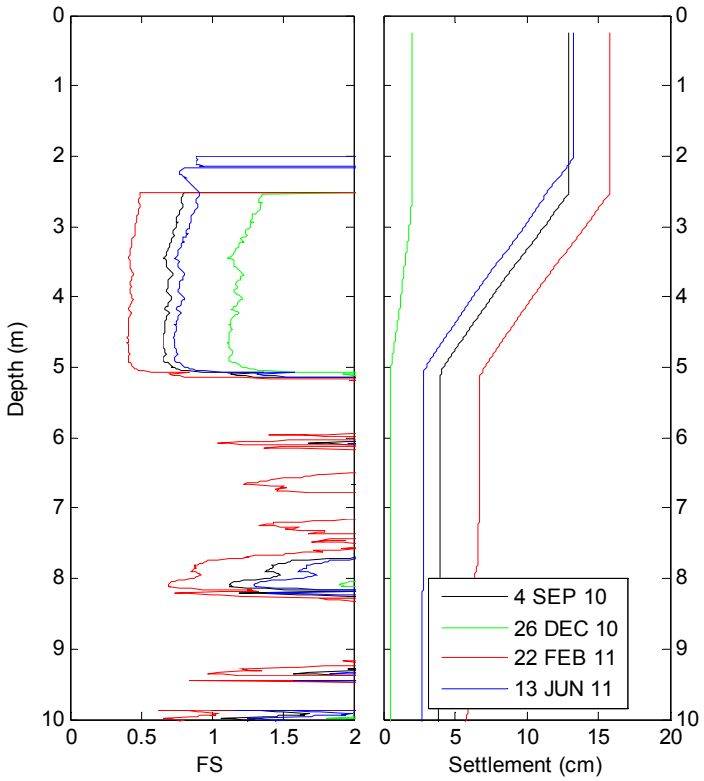

Figure 2.8. FS against liquefaction triggering and settlement due to post-liquefaction volumetric strain profiles at CPT Z4-5 using ZR02-RW98 and PGA_{50} estimates from Bradley and Hughes (2012).

The post-liquefaction residual shear strength of the shallow SM/ML layer was estimated to be 6 kPa to 10 kPa using the Olson and Stark (2002) and IB08 procedures. The bottom of the SE footing adjacent to CPT Z4-5 was at a depth of about 1.3 m. The static bearing capacity of the foundation soils at this location can be estimated using procedures developed for a two-layer cohesive soil deposit (NAVFACDM 7.02 1986). The *FS* against a bearing capacity failure is 2.1 to 2.3 at the location of the SE corner footing, which was judged to be most critical, using the residual shear strength of the shallow liquefiable SM/ML materials and an equivalent undrained shear strength of the SM/ML materials above the groundwater. If the materials above the groundwater lose strength due to the upward migration of liquefied soil, then the *FS* is below one. The SE footing may have underwent a partial bearing capacity failure, but its differential settlement was largely the result of ground loss due to sediment ejecta and some contribution of other settlement mechanisms described by Bray and Dashti (2010), because bulging of the ground surface was not observed at this site.

Liquefaction-induced free-field level ground settlements at the locations of CPTs Z4-5, Z4-7, and Z4-10 were calculated based on the post-liquefaction volumetric strain ZR02-RW98 procedure discussed previously. As is often done in engineering practice, the upper 17 m of the soil deposit was characterized, so liquefaction-induced settlement estimates due to volumetric strains over this thickness were calculated and summarized in Table 2.3. Settlements due to post-liquefaction volumetric strains increase significantly when the shallow SM/ML layer exists beneath the groundwater table as it does in CPT Z4-5, which is at the SE corner of the building.

Free-field vertical settlements due to post-liquefaction volumetric strains suggest a differential settlement of about 6 cm across the building due to the Christchurch earthquake. However, the building actually settled differentially 25 cm more at its south end than at its north end for this event. Ground loss under the shallow foundations due to sediment ejecta likely led to larger settlements. Moreover, shear-induced mechanisms such as SSI-ratcheting likely contributed to larger settlements at the SE corner of the CTUC building. Liquefaction of soils below a depth of 8 m contributed significantly to the amount of calculated settlement, but their impact on the building performance was relatively minor.

Table 2.3. Calculated surface settlements at CPT locations near the CTUC Building. Settlements are due to post-liquefaction volumetric strains in the top 17 m and based on median *PGA* estimates.

CPT ID	Reconsolidation Settlement (cm)			
	4 SEP 10	26 DEC 10	22 FEB 11	13 JUN 11
Z4-5	13	2	16	13
Z4-7	2	0	10	1
Z4-10	2	0	7	1

Whereas the ZR02-RW98 procedure underestimated liquefaction-induced building settlement due to the Christchurch earthquake, it overestimated the observed settlement for the Darfield and June 2011 events. Liquefaction triggering evaluation procedures are typically conservative. The calculation of $FS_l < 1.0$ for the Darfield earthquake leads to a post-liquefaction settlement at CPT Z4-5 that is close to that calculated for the Christchurch earthquake due to the sensitivity of the ZR02 procedure when FS_l is near one. Severe liquefaction and significant damage were observed for the latter event, but not for the former event, so commonly used procedures are not be able to discriminate between these two events for this case. Post-liquefaction settlement estimates provide a rough index of seismic performance and engineering judgment is required in interpreting their results.

Analyses were also performed with the ZR02-IB08 procedure described previously to evaluate the sensitivity of post-liquefaction ground settlements to the method used to calculate FS_l. Unlike the RW98 method that accounts for grain characteristics with I_c, the IB08 method requires an estimate of a soil's *FC*. The recommended general I_c-*apparent FC* correlation presented by RW98 tends to underestimate the actual *FC* for a given I_c when $I_c > 1.9$ (corresponding to $FC > 10\%$) for the Christchurch soils (Taylor et al. 2012). In addition to their general correlation, RW98 also present a curve for $PI < 5\%$ soils and warn that these correlations are approximate due to the dependency of I_c on plasticity, mineralogy, sensitivity, and stress history. The IB08 liquefaction triggering correlation is most sensitive to *FC* when the *FC* is between 10% and 30%. The RW98 general correlation underestimates *FC* and their PI < 5% curve overestimates *FC* for Christchurch soils over this range. The RW98 recommended general correlation is used in this study to estimate *FC* in the absence of site-specific laboratory test data, because its use in the IB08 procedure is conservative and more common. Further work is required to refine the I_c-*FC* correlation for Christchurch soils.

2.7.2 SA Building in Zone 8

The SA Building (S43.5252 E172.6419) was located about 200 m NW of the Avon River and was a two-story RC frame structure with concrete infilled walls, interior timber-framed walls, and timber flooring that was 15 m by 30 m in plan with two bays in the E-W direction and six bays in the N-S direction. The building was remodeled in 1997-98, during which time the two southernmost first floor bay frames were removed to create an exterior parking area and replaced with a more robust RC frame. In addition, several of the pre-existing frames were retrofitted with steel K-bracing. It appears that the original building was founded on a grid of shallow strip footings that were approximately 0.5 m wide and 0.6 m deep. The new shallow square footings within the southernmost two bays were either 1.5 m by 1.5 m or 3.3 m by 3.3 m and were 0.6 m thick. The footings were cast in place under the pre-existing foundation tie beams at a depth of approximately 1.4 m below the ground surface.

Liquefaction occurred at the site during the Darfield earthquake (Ruamoko Solutions 2010). While it was judged that there was no significant damage to the building's primary structural system from this event, there was sediment ejecta observed at the ground surface around the building perimeter and in the elevator shaft. Post-event inspections revealed ground cracks and surface depressions at the site, along with a "bulge" at the front of the building that they judged was likely caused by upward moving liquefied sediment that was trapped by an overlying, well compacted, surface layer. Minor amounts of fresh sediment ejecta were also observed around the building perimeter following the June 2011 earthquake.

Liquefaction was far more severe and damaging during the Christchurch earthquake. Figure 2.9 illustrates severe ground cracking in the road south of the building and the extent of the ejected groundwater pond near the entrance of the building, which was reported to be 0.5 m deep, as well as the extent of liquefaction just north of the building. The building was surveyed by UCB-UC researchers in March 2011 and again in July 2011. During the March 2011 survey, Cubrinovski et al. (2011a) observed nearly continuous sediment ejecta around the perimeter of the building and evidence of its foundation displacing downward into the surrounding ground with the ground floor at the south entrance of the building uplifted and blistered. The building settled approximately 25 cm relative to the surrounding ground at its SE corner and approximately 10-20 cm at its NW corner. Due to this damage, the building was demolished in 2012.

Figure 2.9. (a) Views of the south end and (b) north end of SA Building taken approximately 2 hours after the Christchurch earthquake. (c) Photo of the east side of the building taken June 5th, 2011. (Photos courtesy of Shipleys Audiovisual Ltd.)

Three CPTs were performed at the SA Building site. The subsurface conditions along the length of the building are illustrated in Fig. 2.10. The site consists of a shallow SM/ML layer to a depth of 2-2.5 m with $q_t < 5$ MPa and $2<I_c<2.5$ similar to the shallow SM/ML layer observed at the CTUC and Armagh-Madras sites, which is underlain predominantly by sand and silty sands (SP/SM) until refusal was encountered. Tip resistance in the lower SP/SM unit was variable and was occasionally less than 10 MPa. The groundwater depth at the SA site was about 1.5 m throughout the Canterbury earthquake sequence (T&T 2012).

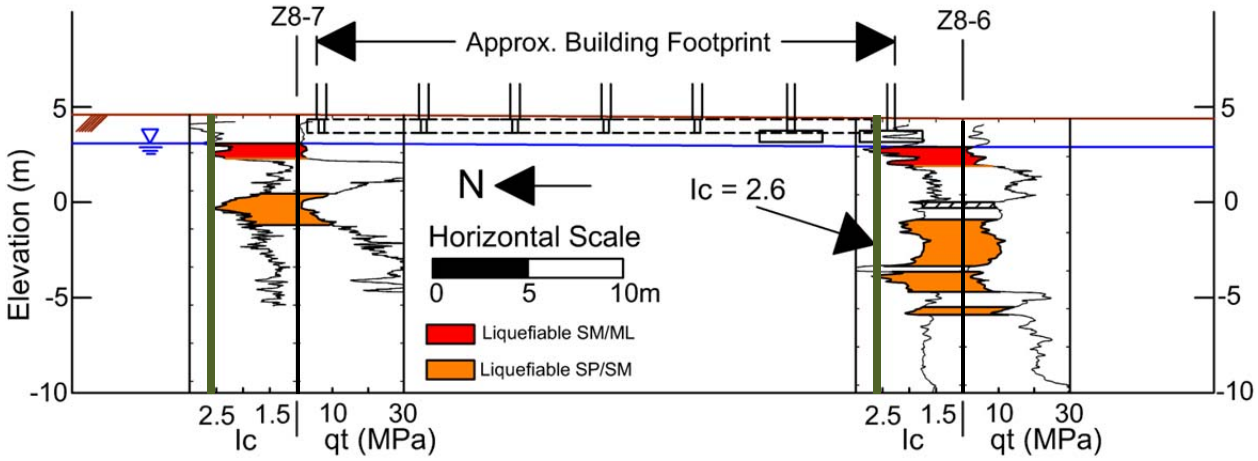

Figure 2.10. Subsurface conditions at SA site showing zones of materials with $FS_l < 1.0$ based on the RW98 procedure using PGA_{50} from Bradley and Hughes (2012) for the Christchurch earthquake.

Zones of materials with $FS_l < 1.0$ using the median PGA during the Christchurch earthquake are also indicated in Fig. 2.10. Consistent with previous evaluations, the critical liquefiable layer is the shallow SM/ML unit when below the water table. There are also layers of liquefiable materials in the underlying SP/SM unit. The calculated FS_l profiles for all four events at CPT Z8-7 are presented in Fig. 2.11 using the median PGA estimates. The *FS* against bearing failure was calculated using the procedures described previously. It is likely that the *FS* against bearing capacity failure was near or below 1.0 at the southern end of the building due to the weakened state of the liquefied shallow SM/ML materials. Consequently, a bearing capacity failure mechanism likely contributed to the observed foundation punching, though the effects of ground loss due to sediment ejecta were clearly evident and other displacement mechanisms noted in Bray and Dashti (2010) could have also occurred.

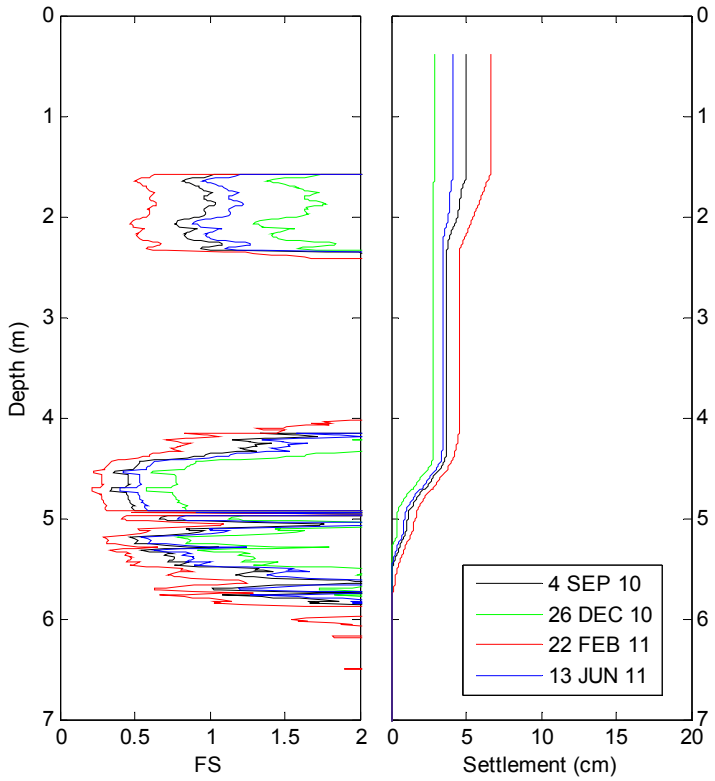

Figure 2.11. FS against liquefaction triggering and settlement due to post-liquefaction volumetric strain profiles at CPT Z8-7 using ZR02-RW98 and PGA_{50} estimates from Bradley and Hughes (2012).

The free-field, level ground settlement estimates due to post-liquefaction volumetric strains over the upper 10 m of the soil deposit using the ZR02-RW98 procedure are summarized in Table 2.4. Once again, the calculated settlements during the Christchurch earthquake are not much higher than those for the Darfield and June 2011 events. The settlements calculated at CPT Z8-11 are low for all events, because the layer of liquefiable SP/SM materials observed at depths between 4 and 4.5 m at CPTs Z8-6 and Z8-7 was not present at Z8-11. Significant amounts of sediment ejecta were observed in the vicinity of CPT Z8-11 after the Christchurch earthquake, and the building underwent a punching failure in this area. Whereas the only liquefiable materials in the upper 7.3 m at this location appear to be the 0.7 m-thick shallow SM/ML materials, the observed sediment ejecta and building punching indicate that the effects of liquefaction of these materials were far more severe than what is suggested using post-liquefaction volumetric reconsolidation procedures intended for free-field applications. These procedures give equal emphasis to liquefaction-induced volumetric strains throughout the soil profile, when in fact, liquefaction-induced movements of shallow foundations are dominated by shallow soil layers that liquefy, especially if these soils are removed beneath the foundation through the development of sediment ejecta.

Table 2.4. Calculated surface settlements at CPT locations near the SA Building. Settlements are due to post-liquefaction volumetric strains in the top 10 m and based on median *PGA* estimates.

CPT ID	Reconsolidation Settlement (cm)			
	4 SEP 10	26 DEC 10	22 FEB 11	13 JUN 11
Z8-6	5	1	9	3
Z8-7	5	3	7	4
Z8-11*	2	0	2	1

* Refusal was encountered at a depth of 7.3m

2.7.3 Building Group in Zone 1

There were three multi-story buildings with different foundation types located close to each other in Zone 1. The building sites liquefied significantly during the Christchurch earthquake. They are located within an area marked as an old stream channel on the "Black Maps" (Cubrinovski et al. 2011a). Localized areas of minor-to-moderate liquefaction occurred during the Darfield and June 2011 earthquakes. Photographs of the buildings are shown in Fig. 2.12, and the site plan shown in Fig. 2.13 depicts the buildings and adjacent buildings with the locations of CPTs and boring.

The "PILE-6" Building (S43.5268 E172.6386) was a six-story frame structure that was 18 m wide in the E-W direction and 34 m long in the N-S direction. Two CPTs and one borehole were performed in 1987 before the building was constructed (see Fig. 2.13, Soils and Foundations 1987) and revealed very loose to loose sands, silty sands, and sandy silts to a depth of 12 m, with another loose layer under the northern part of the site between depths of 15 m and 17 m. The groundwater table was encountered at a depth of 2 m. The geotechnical consultant noted that much of the soil profile was liquefiable and recommended a mat foundation in combination with ground improvement or a pile foundation with toe depths of 12-14 m or 18 m, depending on local variations in the soil conditions. The constructed building's foundation consisted of 275 mm square piles interconnected with grade beams.

Figure 2.12. Zone 1 Building Group: (a) PILE-6, (b) FTG-7, and (c) FTG-4 buildings.

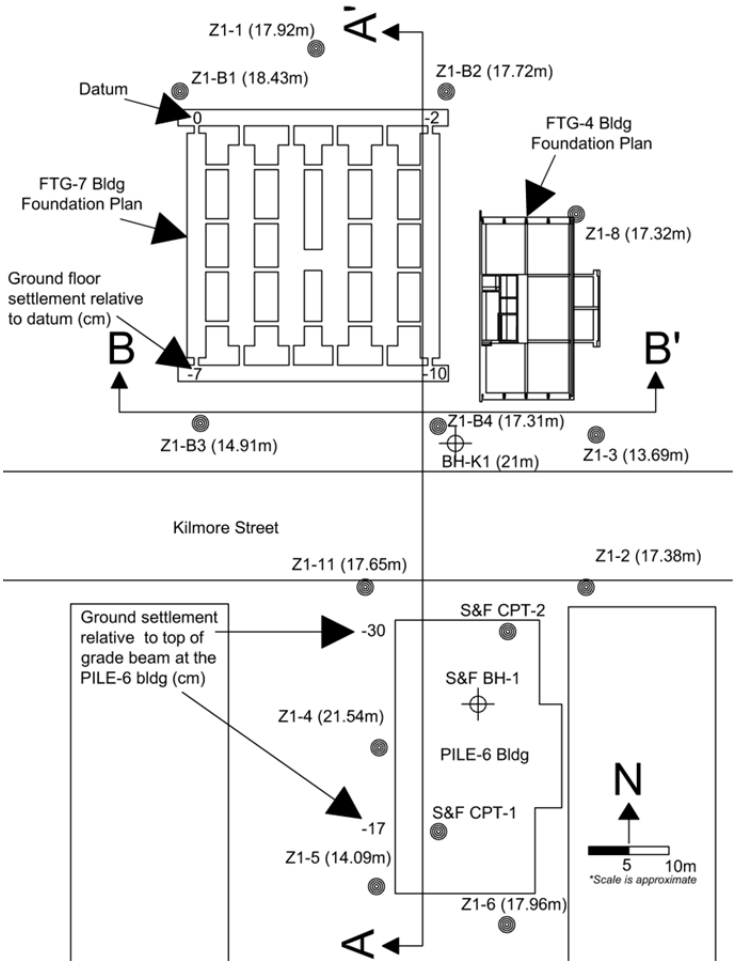

Figure 2.13. Zone 1 CPT locations, and shallow foundation plans for FTG-7 and FTG-4 buildings.

The "FTG-7" Building (S43.5263 E172.6384) was a seven-story steel-framed structure (approved in 1987) that was 29 m wide in the E-W direction and 32 m long in the N-S direction and located across the street from the PILE-6 Building. Its foundation consisted of shallow RC strip footings, between 2 m and 3.3 m wide and 0.6 m deep, interconnected with square RC tie beams that had a cross sectional area of 0.36 m^2 (Fig. 2.13). The base of the perimeter strip footings was 1.2 m deep, and the base of the interior strip footings was 0.7 m deep. The first floor perimeter wide-flange steel columns of the building were encased in concrete. The ground floor consisted of 10 cm-thick unreinforced concrete and floors two through seven consisted of 12 cm-thick RC over 0.75 mm galvanized steel decking. The exterior walls were composed of pre-cast RC wall panels.

The "FTG-4" Building (S43.5263 E172.6387) was a four-story RC framed structure (approved in 1972) that was 15 m wide in the E-W direction and 23 m long in the N-S direction and located adjacent to the FTG-7 Building. Its foundation consisted of shallow RC strip footings interconnected with square RC tie beams with a cross-sectional area of 0.09 m^2. The strip footings were typically between 0.6 and 0.85 m wide and 0.35 and 0.6 m thick. In addition to the RC framing elements, the structure also contained parallel concrete block walls that extended from the floor to the roof (approximately 12.2 m), which were oriented in the N-S direction along the eastern and western edges of the building. Floor slabs consisted of 10 cm-

thick concrete for the ground floor and 12 cm-thick RC for the upper floors.

Twelve CPTs and one borehole were performed in the vicinity of these buildings (Fig. 2.13). The log of borehole K1 was previously presented in Fig. 2.3, along with the profile of the adjacent CPT Z1-B4. Figures 2.14 and 2.15 present the corrected cone tip resistance and soil behavior type index profiles based on the CPTs performed along cross sections A-A' and B-B', respectively. While there is some variability in the ground conditions, the shallow subsurface generally consists of two predominant units: a) silty sands and sandy silts with q_t generally less than 5 MPa and I_c generally between about 2.0 and 2.5, and b) sands and silty sands with q_t generally less than 10 MPa and I_c generally between about 1.5 and 2.0. The groundwater depth was about 2.0 m throughout the earthquake sequence (T&T 2012).

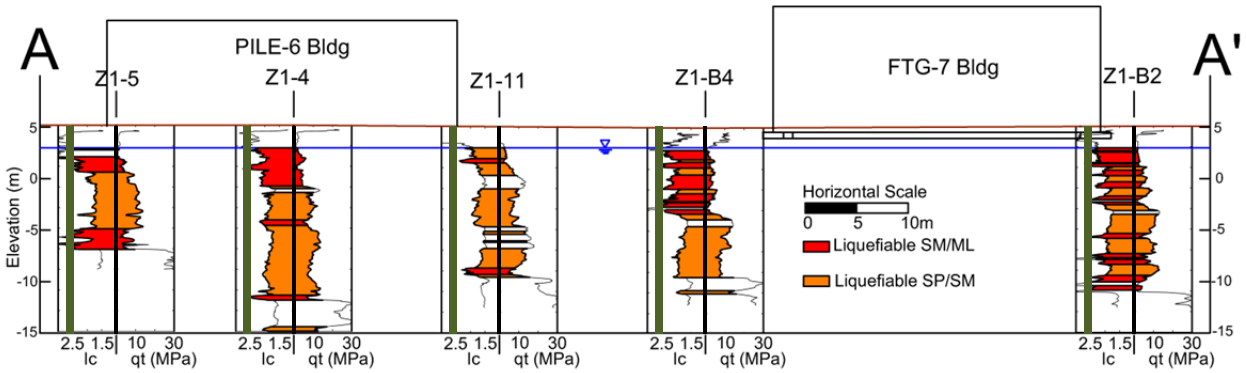

Figure 2.14. Subsurface conditions along section A-A' showing zones of materials with $FS_l < 1.0$ based on the RW98 procedure using PGA_{50} from Bradley and Hughes (2012) for the Christchurch earthquake.

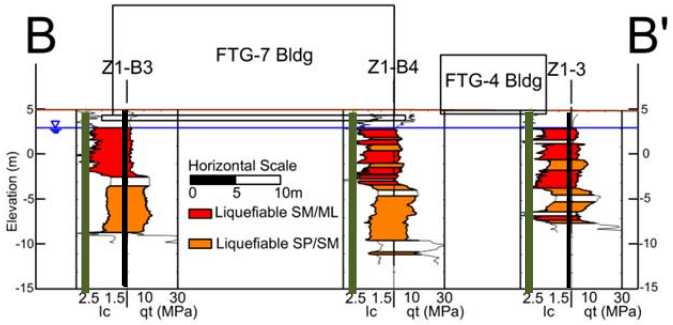

Figure 2.15. Subsurface conditions along section B-B' showing zones of materials with $FS_l < 1.0$ based on the RW98 procedure using PGA_{50} from Bradley and Hughes (2012) for the Christchurch earthquake.

Zones of materials with $FS_l < 1.0$ using the median PGA during the Christchurch earthquake are also indicated in Figs. 2.14 and 2.15. Significant liquefaction is calculated throughout much of the soil deposit for the Christchurch event. The *FS* against bearing failure was calculated using the procedures described previously, and the *FS* were estimated to be 1.4 for the southern strip footing of the FTG-7 Building and 2.8 for the strip footing supporting the eastern block wall of the FTG-4 Building. The free-field, level ground settlement estimates due to post-liquefaction volumetric strains over the upper 14 m of the soil deposit using the ZR02-RW98 procedure are summarized in Table 2.5. Significant settlements are estimated at most CPT locations as a result

of the Darfield, Christchurch, and June 2011 events. Smaller, but non-zero, liquefaction-induced ground settlements are also calculated for the December 2010 event.

Table 2.5. Calculated surface settlements at CPT locations in Zone 1. Settlements are due to post-liquefaction volumetric strains in the top 14 m and based on median *PGA* estimates.

CPT ID	Reconsolidation Settlement (cm)			
	4 SEP 10	26 DEC 10	22 FEB 11	13 JUN 11
Z1-B2	21	5	28	15
Z1-B3	17	6	24	14
Z1-B4	28	13	32	26
Z1-3	16	4	22	12
Z1-4	19	3	26	14
Z1-5	7	1	14	4
Z1-11	16	4	21	13

The ground settled approximately 30 cm and 17 cm relative to the north and south sides, respectively, of the PILE-6 Building during the Christchurch earthquake (Cubrinovski et al. 2011a). Post-liquefaction volumetric reconsolidation settlements were calculated to be 21 cm, 26 cm, and 14 cm at the building's north end (CPT Z1-11), center (CPT Z1-4), and south end (CPT Z1-5), respectively, during the Christchurch earthquake using the ZR02-RW98 procedure. Assuming the pile-supported building did not settle significantly, ground settlements are slightly underestimated for the Christchurch earthquake. Conversely, ground settlements are overestimated for the Darfield earthquake. Despite the substantial ground settlements around the building, the first-story structural frame did not show significant damage.

The FTG-7 Building, however, was damaged significantly with evidence of damage to the structural columns at the ground level. A floor level survey performed in March 2011 indicated approximately 10 cm of settlement of the SE corner of the building relative to the datum at its NW corner (Eliot Sinclair and Partners Ltd. 2011), and a subsequent building verticality survey (Beca 2011) confirmed the building was tilted to the S-SE. Relative settlements of the corners of the ground floor are indicated on Fig. 2.13. Post-liquefaction volumetric reconsolidation settlements from the Christchurch earthquake were calculated to be 25 cm at CPT Z1-B1, 28 cm at CPT Z1-B2, 24 cm at CPT Z1-B3, and 32 cm at CPT Z1-B4. Based on the observations of the settlement of the ground relative to the PILE-6 Building across the street, these estimates appear to be reasonable. However, the ground floor level survey indicated 7 cm of relative settlement of the SW corner (CPT Z1-B3) of the building to its NW corner (CPT Z1-B1). This differential settlement would not be estimated based on a direct comparison of the settlements calculated at CPT Z1-B1 and CPT Z1-B3.

The FTG-4 Building was damaged significantly. A large amount of sediment ejecta was observed in the parking lot behind the building and in front of the building, as well as around and within the building footprint. The strip footings supporting the side block walls settled relatively more than the remainder of the building and the concrete slab on the ground floor was bowed up in the middle. Cracking was observed in several of the exposed concrete columns and in the concrete fascia on the north end of the building. The ground floor slab settled approximately 16 cm more at the building's NW corner than at its NE corner. Post-liquefaction volumetric

reconsolidation settlements during the Christchurch earthquake were calculated to be 22 cm at both CPTs Z1-3 and Z1-8.

Thus, the three buildings in Zone 1 performed differently as a result of being located in an area of severe liquefaction during the Christchurch earthquake. The pile-supported building was comparatively less damaged than the two buildings that were supported on shallow foundations, though access to it was limited due to the significant settlement of the ground that surrounded it. The taller, but wider, FTG-7 Building, underwent less differential settlement than the shorter and narrower FTG-4 Building. The increased plan area of the FTG-7 Building foundation may have also contributed to it undergoing less differential settlement than the FTG-4 Building. Post-liquefaction estimates of ground settlement were reasonable for level ground settlement near the PILE-6 Building, which likely did not settle significantly, for the Christchurch earthquake. However, settlements were underestimated for the June 2011 earthquake and overestimated for the Darfield earthquake. Post-liquefaction volumetric strain-based methods do not capture the settlement of the buildings supported on shallow foundations, which also underwent shear-induced settlement and settlement due to ground loss from sediment ejecta. Moreover, post-liquefaction reconsolidation procedures should not be employed directly to estimate differential building settlement as is sometimes done in engineering practice.

2.8 Findings

The Canterbury earthquake sequence produced varying degrees of liquefaction with differing effects on buildings with different structural and foundation systems. The CPT proved to be a useful site characterization tool when shallow dense gravels were not present. Its results enabled liquefaction triggering evaluations using prevalent procedures that were conservative. The conservatism in the liquefaction triggering assessments led to post-liquefaction ground settlement estimates that were generally similar for the large events in the Canterbury earthquake sequence, whereas significant building settlements and damage in the CBD were observed for the Christchurch earthquake but not for other earthquakes, such as the Darfield and June 2011 events. Moreover, the liquefaction-induced ground settlement procedures do not capture important shear-induced deformation mechanisms, such as SSI ratcheting and partial bearing failure, and the effects of ground loss due to sediment ejecta. Performance-based earthquake engineering requires improved procedures to discern between the differing levels of performance observed in Christchurch during the Canterbury earthquake sequence. Given the brittle nature of the liquefaction phenomenon as soil transforms from a stiff to a soft response rapidly as the excess pore pressure rises beyond a threshold value, the development of robust design procedures to evaluate the effects of liquefaction on buildings will be challenging. However, the case histories provided by the Canterbury earthquake sequence provide a comprehensive set of ground and building performance data for developing such methods.

3. EARTHQUAKE PERFORMANCE OF UNDERGROUND LIFELINES IN CHRISTCHURCH, NZ

3.1 Introduction

In this section, the system-wide aspects of pipeline response are investigated by analysis of the spatially distributed transient and permanent ground deformation (TGD and PGD, respectively) generated by successive earthquakes in the Christchurch area and their effects on the water, wastewater, and gas distribution systems. The data collected for the earthquake sequence are unprecedented in size and detail, involving ground motion recordings from scores of seismograph stations, high resolution light detection and ranging (LiDAR) surveys of the ground surface before and after each main seismic event allowing vertical and lateral ground surface movements to be calculated, and detailed repair records for thousands of km of underground pipelines with coordinates for the location of each repair. This section presents the results of analyses with geographical information systems (GIS) of pipeline performance during the Canterbury earthquake sequence. Pipeline repair rates (RRs), expressed as repairs/km, for different types of pipe are evaluated relative to peak ground velocity in areas not affected by liquefaction. For areas affected by liquefaction, RRs are assessed relative to differential ground surface settlement and ground surface lateral strain, calculated from LiDAR data acquired before and after each main seismic event. Pipeline performance in the gas, water, and wastewater distribution systems are compared, and lessons learned regarding the earthquake performance of underground lifeline systems are summarized.

3.2 Canterbury Earthquake Sequence and GIS Database

Figure 3.1 presents a map of the Canterbury region with causative faults, moment magnitudes (M_Ws), and epicenters for the 7.1 M_W 4 Sept. 2010 Darfield, 6.2 M_W 22 Feb. 2011 Christchurch, 6.0 M_W 13 June 2011, and 5.9 M_W 23 Dec. 2011 earthquakes, as provided by GNS Science (2011). The 6.0 M_W June 13, 2011 earthquake was preceded by a 5.3 M_W event, and the 5.9 M_W 23 Dec. 2011 earthquake was followed by a 5.8 M_W event. Each earthquake resulted in widespread liquefaction damage with substantial damage to underground water and wastewater pipelines in the Christchurch area. This section focuses on the 22 Feb. 2011 and 13 June 2011 earthquakes.

Geospatial data in the form of GIS maps of the Christchurch water and wastewater distribution systems, locations of pipeline repair, and areas of observed liquefaction effects were integrated into a master GIS file. For the water supply this study focuses on damage to water mains, which are pipelines with diameters typically between 75 and 600 mm, conveying the largest flows in the system. The results of systematic visual mapping of liquefaction and lateral spreading provided by CERA (2012) were used, hereafter referred to as zones affected by liquefaction or liquefaction zones. Geocoded data files for approximately 1700 and 1900 km of water and wastewater distribution pipelines, respectively, as well as the repairs associated with each earthquake, were provided by the Stronger Christchurch Infrastructure Rebuild Team (SCIRT). GIS maps were developed showing areas of the pipeline systems and repairs both inside and outside liquefaction zones.

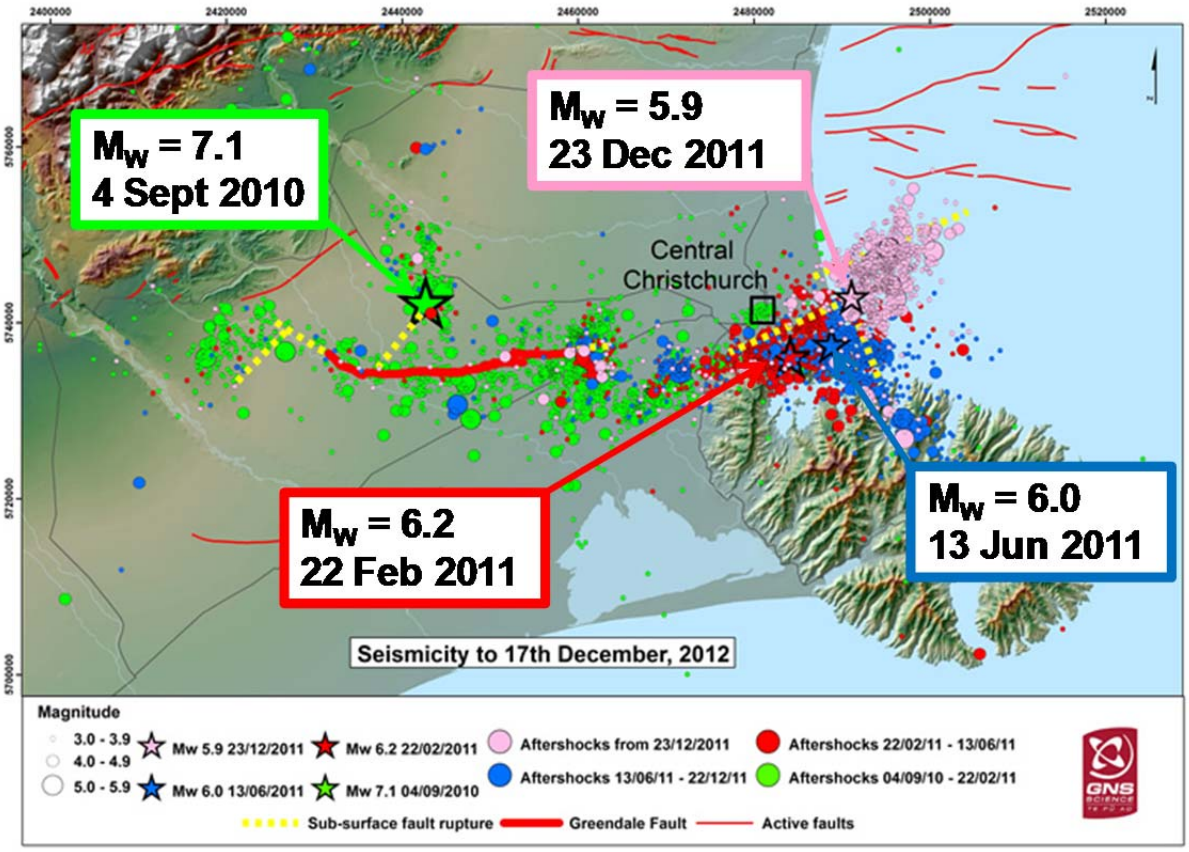

Figure 3.1. Principal earthquakes of the Canterbury earthquake sequence (GNS Science, 2013).

3.3 Pipeline Repair Databases

The water supply repair database provided by SCIRT provides continuous daily repair records for return of services covering the period from February 23, 2011 to May 14, 2012, during which the 13 June 2011 and 23 December earthquakes and numerous aftershocks occurred. Figure 3.2a presents the daily repairs for mains and submains as a function of time. Submains are pipelines with diameter less than 75 mm, which branch off mains to provide water to a limited number of houses. Also shown in the figure are the two large earthquakes and select aftershocks. Figure 3.2b shows the cumulative frequency of main repairs, derived from Fig. 3.2a, from the time of the 22 Feb. 2011 earthquake to just before the 13 June 2011 earthquake. It can be seen that the initial frequency of repairs is very high and reduces through a transitional phase to a steady state rate of repair, leading up to the 13 June 2011 earthquake. A similar pattern of repairs is shown by the cumulative frequency distribution after the 13 June 2011 earthquake, with initial, transitional and post-earthquake steady state repair conditions identified in Fig. 3.2c.

The time at the start of the steady state repair conditions is used as the end of repair activities directly related to the large earthquakes. Thus, the number of repairs and specific records of repairs attributable to the 22 Feb. and 13 June 2011 earthquakes were taken from repair records between the day after the earthquake and the beginning of the steady state repair period.

Figure 3.2d shows the daily and weekly average (expressed as a daily rate) repairs for the steady state conditions after the 13 June 2011 earthquake. For comparison, the Christchurch

average pre-earthquake (Christchurch City Council, 2006) and average US water distribution system (Bardet et al, 2010) daily repairs are shown in the figure. It can be seen that the steady state repair rate after large earthquakes in Christchurch is approximately 3 to 4 times greater than the rates not affected by prior earthquakes.

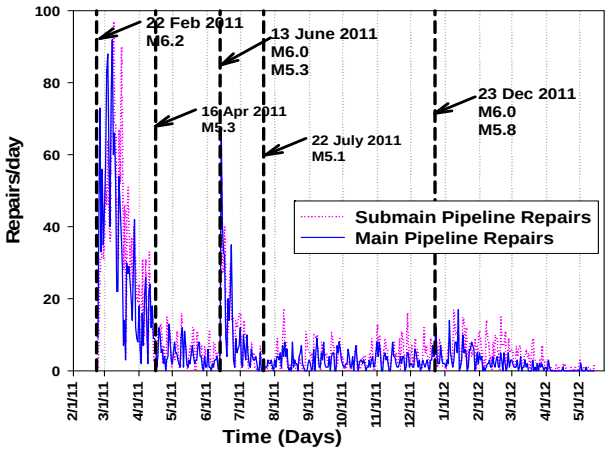

a) Daily main and submain repairs

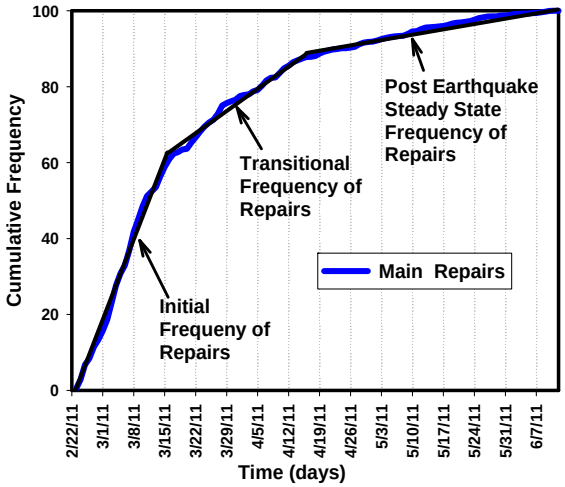

b) Cumulative frequency of repairs between 22 Feb. and 13 June 2011

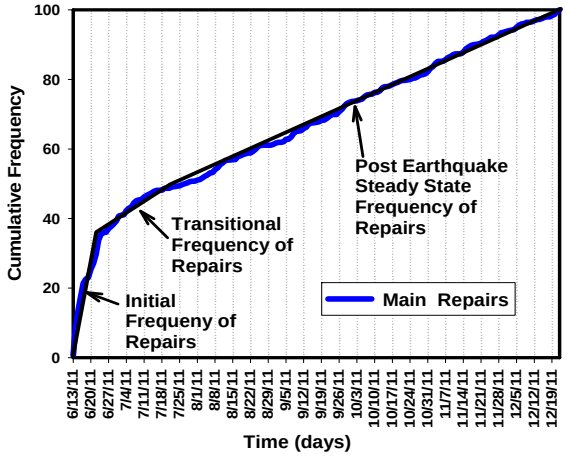

c) Cumulative frequency of repairs between 13 June and 23 Dec. 2011

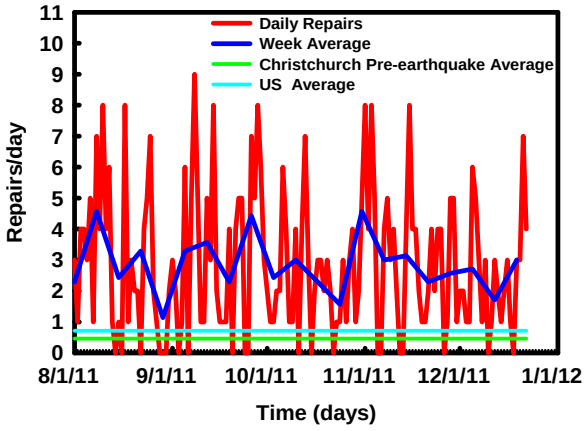

d) Observation of repairs in post-earthquake steady state stage

Figure 3.2. Water distribution repair characteristics with respect to time.

Figures 3.3a and 3.3b are plots similar to those in Figs. 3.2a through 3.2c from repair records provided by SCIRT for wastewater pipelines for Feb. 23, 2011 to May 14, 2012. Figure 3.3a presents the daily repairs for wastewater pipelines as a function of time. Figure 3.3b shows the cumulative frequency of repairs for reinstatement of services, derived from Fig. 3.3a. Similar to the trends in Figs. 3.2b and 3.2c there is a steady state of repairs that is used to identify the end of repair activities directly related to the 22 Feb. and 13 June 2011 earthquakes.

In contrast to the trend in Fig. 3.2b, significant numbers of repairs were not recorded until 3 to 4 weeks after the 22 Feb. 2011 earthquake. This delay is related to the repair efforts that were first concentrated on the water supply, leaving a smaller work force to attend to the wastewater system until substantive water supply repairs were achieved. Because wastewater system repairs

were preceded by removal of debris washed into damaged pipes and closed circuit television (CCTV) inspection of the lines, the rate of repairs increased slowly at first. As can be seen in Fig. 3.3b, the 13 June 2011 earthquake occurred before convergence to a steady state. In contrast to the water supply, it is not possible to identify all wastewater repairs caused by the 22 Feb. 2011 earthquake because many lines damaged by that earthquake had not been repaired when the 13 June 2011 earthquake occurred. It was therefore necessary to develop an averaging procedure for both earthquakes to evaluate wastewater pipeline RRs relative to PGD, as described later in the section.

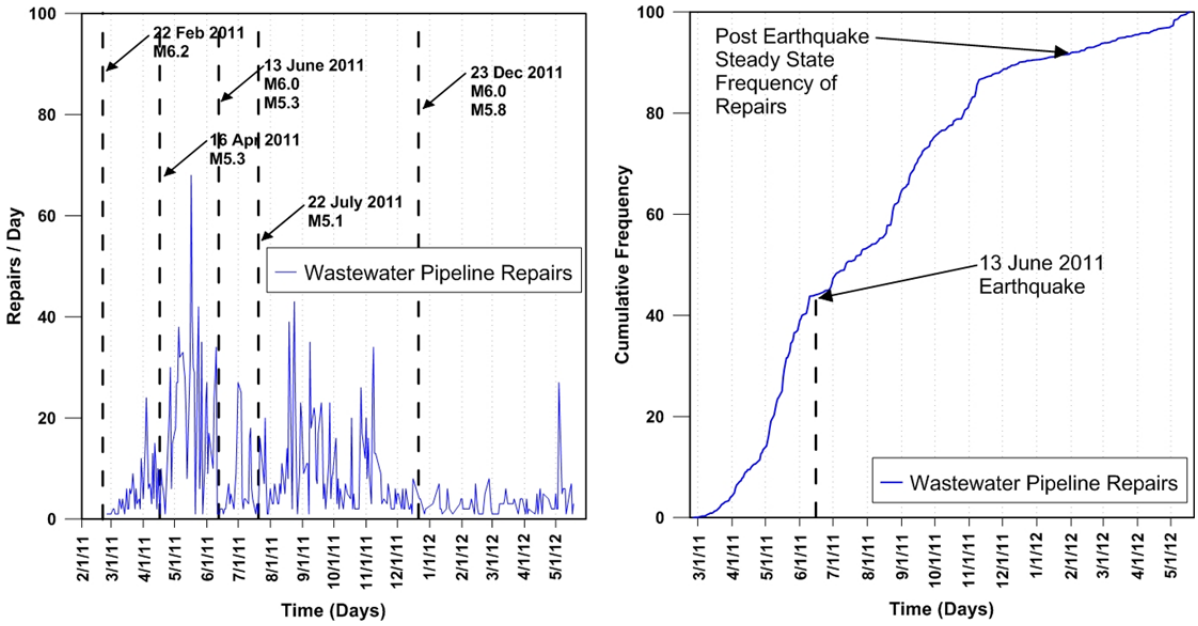

a) Daily wastewater pipeline repairs

b) Cumulative frequency of repairs between 22 Feb. and after June 2011

Figure 3.3. Wastewater distribution repair characteristics with respect to time.

3.4 GIS Evaluation of Water Supply Pipeline Performance

Pipeline performance was evaluated with GIS for RRs 1) outside zones of observed liquefaction effects where TGD is likely to be the primary cause of damage, and 2) inside zones of observed liquefaction, where PGD is likely to be the primary cause of damage. GIS shape files for areas of observed liquefaction effects were obtained from CERA (2012) for the 22 Feb. and 13 June 2011 earthquakes, and expanded to include a zone of influence at the boundaries of the liquefaction areas. Extension of the mapped boundaries of the liquefaction zones is warranted because surface evidence of liquefaction does not capture all the areas affected by liquefaction effects below the ground surface. The zone of influence for pipeline damage beyond the liquefaction area boundaries was taken as 125 m, which is approximately one-half a typical street length in a residential neighborhood and is consistent with the distance that significant pullout forces can be transmitted longitudinally along underground pipelines (e.g., O'Rourke and Liu, 1999).

Using the databases and procedures described above, statistics for water and wastewater pipelines for the Christchurch and 13 June 2011 earthquakes are summarized in Tables 3.1 and 3.2, respectively. The tables provide information for various pipe types pertaining to pipeline length, overall repairs, repairs in liquefied areas, percentage of pipelines in liquefied areas, and RRs inside and outside areas of observed liquefaction for each earthquake. The category of "other" includes pipe types that were individually present in quantities too small for robust statistical analyses. Because RR represents damage normalized by available pipe length, the RRs are a good indicator of relative vulnerability. Small differences in the lengths of various water supply pipe types for each earthquake reflect post earthquake reconstruction and changes in the system.

Data pertaining to asbestos cement (AC), cast iron (CI), polyvinyl chloride (PVC), and modified polyvinyl chloride (MPVC) are summarized for the water supply in Table 3.1. The PVC (for water) and unplasticized polyvinyl chloride UPVC (for wastewater) pipelines are manufactured from unplasticized PVC polymer, and MPVC pipelines are manufactured with additives in the unplasticized PVC polymer to promote greater ductility and resistance to impact. Data pertaining to AC, concrete (CONC), earthenware (EW), UPVC, and reinforced concrete pipe with rubber rings [gaskets] (RCRR) are summarized for the wastewater system in Table 3.2.

As shown in Table 3.1, the RRs for AC and CI pipelines are similar for both earthquakes and approximately 3 to 5 times larger than PVC pipeline RRs, which in turn are 2 to 4 times greater than those of MPVC pipelines. As referenced by RR, damage during the 22 Feb. 2011 earthquake of all pipelines types is generally 10 to 30 times greater in areas affected by liquefaction relative to areas with no observed liquefaction effects.

Table 3.1. Statistics of water pipeline repairs and repair rates in both liquefaction and non-liquefaction areas associated with different water pipe types for the 22 Feb. and 13 June 2011 earthquakes.

Earthquakes	Pipe Material	Pipe Length (km)	Repairs	Overall Average RR	Repairs in LIQ[1] areas	Pipeline in LIQ[1] areas (%)	Average RR in LIQ[1] areas	Average RR in Non LIQ[1] areas
22 February 2011	AC	861.5	1135	1.32	965	47.1	2.38	0.37
	CI	191.6	268	1.40	232	68.3	1.77	0.59
	PVC	208.7	71	0.34	67	53.6	0.60	0.04
	MPVC	149.7	16	0.11	15	32.7	0.31	0.01
	Other	301.3	155	0.51	134	47.1	0.94	0.13
	Total	1712.7	1645	0.96	1413	49.0	1.68	0.27
13 June 2011	AC	857.7	252	0.29	211	46.8	0.53	0.09
	CI	189.4	69	0.36	35	59.2	0.31	0.44
	PVC	204.5	17	0.08	15	54.6	0.13	0.02
	MPVC	149.5	4	0.03	2	35.3	0.04	0.02
	Other	296.1	64	0.22	42	44.6	0.32	0.13
	Total	1697.2	406	0.24	305	47.7	0.38	0.11

[1]LIQ: Areas with observed liquefaction at the ground surface

Table 3.2. Statistics of wastewater pipeline repairs and repair rates in both liquefaction and non-liquefaction areas associated with different wastewater pipe types for the 22 Feb. and 13 June 2011 earthquakes.

Earthquakes	Pipe Material	Pipe Length (km)	Repairs	Overall Average RR	Repairs in LIQ[1] areas	Pipeline in LIQ[1] areas (%)	Average RR in LIQ[1] areas	Average RR in Non LIQ[1] areas
22 February 2011	AC	174.7	58	0.33	34	39.3	0.50	0.23
	CONC	128.0	99	0.77	99	81.0	0.95	0.00
	EW	375.3	434	1.16	399	73.7	1.44	0.35
	UPVC	351.2	19	0.05	17	29.5	0.16	0.01
	RCRR	670.5	299	0.45	271	50.8	0.80	0.08
	Other	190.5	237	1.2	218	42.8	2.67	0.17
	Total	1890.3	1146	0.61	1038	51.6	1.06	0.12
13 June 2011	AC	174.7	37	0.21	30	40.5	0.42	0.07
	CONC	128.0	111	0.87	108	68.4	1.23	0.07
	EW	375.3	357	0.95	299	61.1	1.30	0.40
	UPVC	351.2	16	0.05	10	37.5	0.08	0.03
	RCRR	670.5	229	0.34	205	51.5	0.59	0.07
	Other	190.5	585	3.1	557	38.3	7.64	0.24
	Total	1890.3	1335	0.71	1209	49.6	1.29	0.13

[1]LIQ: Areas with observed liquefaction at the ground surface

As shown in Table 3.2, CONC and EW pipeline RRs are highest for both earthquakes and approximately 2 to 4 times larger than AC and RCRR pipeline RRs, which in turn are 4 to 9 times greater than those for UPVC pipelines. As referenced by RR, damage during both earthquakes to all pipelines types is generally 5 to 15 times greater in areas of liquefaction relative to areas with no observed liquefaction. Overall water and wastewater pipeline RRs are comparable, although AC and UPVC wastewater pipeline RRs for the 22 Feb. 2011 earthquake are relatively low. The lower RRs may be the result of damaged lines that were not repaired at the time of the 13 June 2011 earthquake.

3.5 Pipeline Repair Correlations

Correlations were developed for RR relative to the geometric mean peak ground velocity (GMPGV) to assess TGD effects on the pipelines, and additional correlations were developed for RR relative to differential vertical ground surface movement and lateral ground surface strains. The procedures for developing these correlations and associated regression results are described in this section.

3.5.1 Screening Criteria

The fidelity of the RR statistics is sensitive to the pipeline length sampled and number of repairs observed within a given sampling length. To select lengths sufficient to produce meaningful correlations, models adopted by previous researchers (e.g., Trautmann et al., 1986)

were used in which pipeline damage is assumed to follow a Poisson distribution. Using the approach proposed by O'Rourke and Deyoe (2004) combined with a Poisson distribution, the sampling length criterion is given by

$$(1-\alpha)p \le (RR)x \le (1+\alpha)p \tag{3.1}$$

in which p is the "true" number of repairs; α is a percentage of the true value, p; RR is repair rate; and x is sampling length. For a Poisson distribution, the mean, μ = (RR)x, and the standard deviation, $\sigma = [(RR)x]^{1/2}$.

The probability (i.e., confidence level) that the sampled number of repairs is within ± α of the true value can be determined by recognizing that the sampled repairs will follow a normal distribution in accordance with the central limit theorem. For a confidence interval of β_c and corresponding standard normal deviate, $\Phi^{-1}(\beta_c)$, the lower bound of Eqn. 3.1 is

$$\mu - \varphi^{-1}(\beta_c)\sigma = (1-\alpha)p \tag{3.2}$$

and the upper bound is

$$\mu + \varphi^{-1}(\beta_c)\sigma = (1+\alpha)p \tag{3.3}$$

Combining Eqns. 3.1 through 3.3 with p = (RR)x, results in

$$x \ge {[\varphi^{-1}(\beta_c)]^2}/{\alpha^2(RR)} \tag{3.4}$$

in which x is the sampling length.

This expression expands on the approach of O'Rourke and Deyoe (2004), whereby pipeline damage follows a binomial distribution for a sampling length of 1 km. As the sampling distance decreases, the length converges to the value given by Eqn. 3.4. Pipeline RR data were screened using Eqn. 3.4 with 90% confidence and α = 50%. For example, to select the minimum sampling length for a 90% confidence limit, α = 50%, and RR = 1 repair/km, one determines $\Phi^{-1}(90\%)$ = 1.645 and then uses Eqn. 3.4 to obtain 10.82 km.

3.5.2 Repair Rates For Transient Ground Deformation

As explained by O'Rourke et al. (2012), ground motion records from 50 stations were collected for analysis related to both the 22 Feb. and 13 June 2011 earthquakes, respectively. The GMPGV is the mean of the natural logs of the two maximum horizontal peak ground velocity (PGV) values taken from ground motion recordings available from GNS Science (Geonet, 2011) at each station. The spatial distribution of GMPGV was estimated from recorded ground motions, using ordinary kriging with a spherical variogram, as described by Jeon and O'Rourke (2005) for PGV spatial analyses of the 1994 Northridge earthquake.

Figure 3.4 shows the zones of observed liquefaction, water supply pipelines, repairs outside liquefaction zones, and contours of GMPGV for the 22 Feb. 2011 earthquake, pertaining to AC and CI distribution mains, respectively. The areas of observed liquefaction are shown in white,

and the pipelines and pipeline repairs outside liquefaction zones are displayed throughout the GMPGV contours. The figures provide a conceptual basis for the data screening process. To correlate pipeline RR with GMPGV, for example, one identifies pipelines of a particular type and associated repairs outside the liquefaction areas in conjunction with the estimated GMPGV. With GIS, this correlation process is automated and performed numerically. Using the GIS database of pipelines and repair locations, the repair rate (RR) for a given range of GMPGV was calculated by dividing the number of repairs for a particular type of pipeline by the kilometers of that pipeline type within a contour interval of 10 cm/s. A similar process was followed for areas of observed liquefaction, as described later in the section.

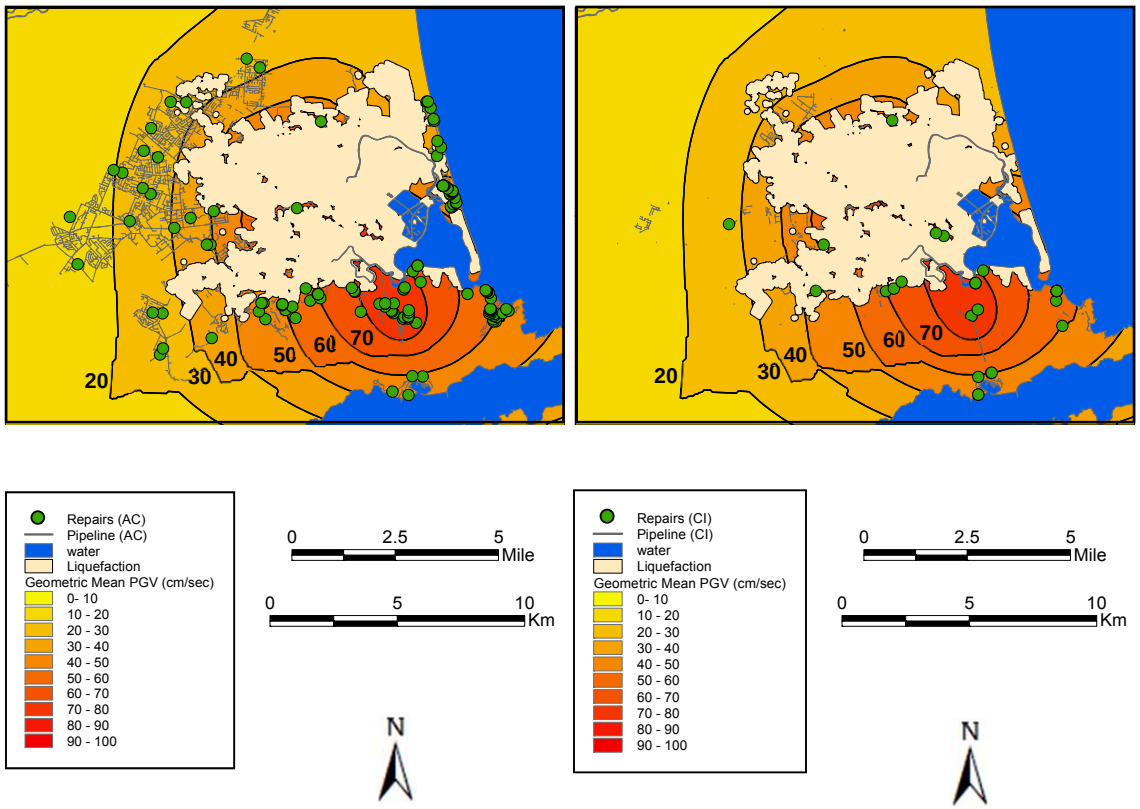

(a) (b)

Figure 3.4. a) 22 Feb. 2011 earthquake AC pipeline layout and repairs; map of GMPGV is the background. b) 22 Feb. 2011 earthquake CI pipeline layout and repairs; map of GMPGV is the background.

Using the Eqn. 3.4 screening criteria, RRs for AC pipelines and various GMPGVs were obtained for the 22 Feb. and 13 June 2011 events, and combined with similar data reported by Jeon (2002) for AC pipelines damaged by the 1994 Northridge earthquake. The results are presented in Fig. 3.5a. The linear regression for all earthquakes is statistically robust with r^2 = 0.92 and balanced distribution of residuals. Using similar techniques for CI pipelines, three data points for Christchurch are combined with worldwide data reported by Jeon and O'Rourke

(2005) to develop the linear regression in Fig. 3.5b. The Christchurch data are for relatively high GMPGVs, and plot slightly above the linear trend for previous earthquakes.

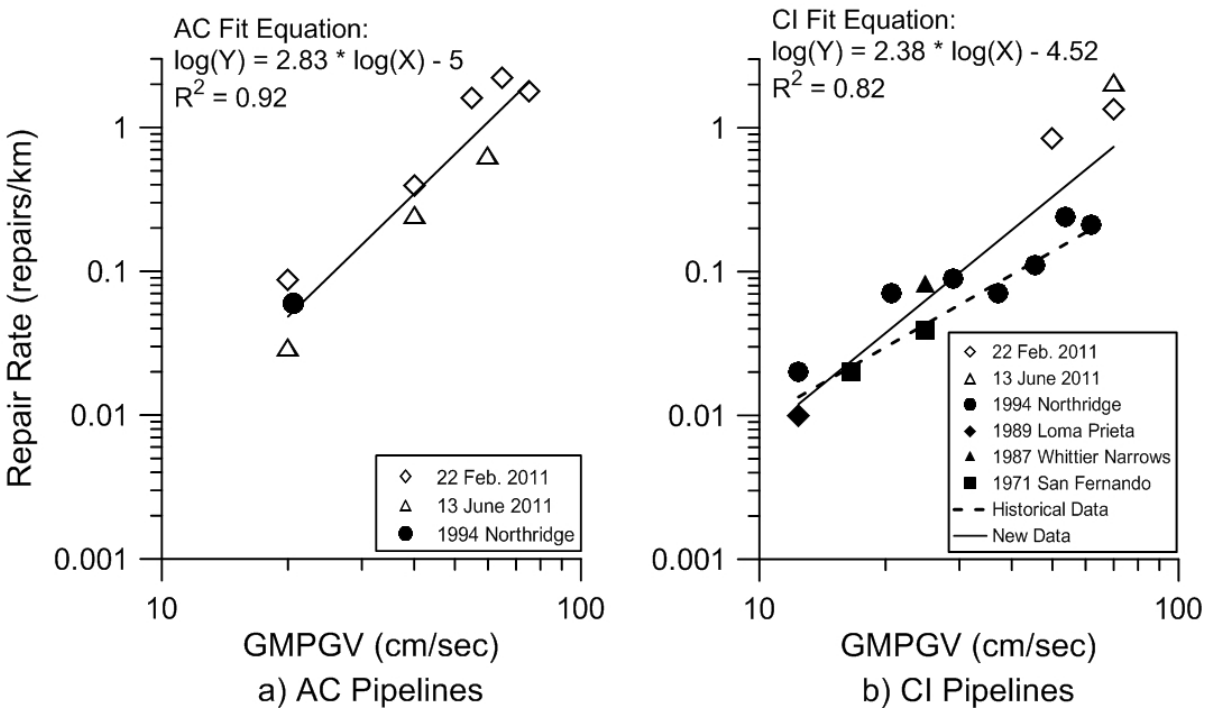

Figure 3.5. Repair rate vs. GMPGV for a) AC pipelines and b) CI pipelines.

To develop RR correlations for differential vertical ground surface movement in zones of observed liquefaction, high resolution LiDAR survey data, available through the Canterbury Earthquake Recovery Authority [CERA] (2012), were used. The LiDAR surveys were flown before and after each earthquake. Each LiDAR survey produces an elevation surface. The accuracy of the vertical LiDAR survey data is between ± 70 mm and ± 150 mm (CERA, 2012). Change in elevation surfaces (also known as vertical settlement surfaces) were derived by subtracting the LiDAR elevation surfaces before and after an earthquake.

Figure 3.6 shows the area where vertical ground surface movement was calculated based on the overlapping area of the pre and post earthquake LIDAR survey extents for the 22 Feb. 2011 earthquake superimposed on the areas of observed liquefaction. The pipeline system and repair locations are also presented in the figure. Correlations of RR with differential vertical movement were developed for the intersection of the areas of observed liquefaction and the areas with calculated vertical ground surface movement, as illustrated in the figure.

Angular distortion, β, is defined as the differential vertical movement between two adjacent LiDAR points ($d_{v1} - d_{v2}$) divided by the horizontal distance, l, separating them, such that $\beta = (d_{v1} - d_{v2})/l$. It is used in this work to evaluate the effects of differential vertical movement on pipeline damage. There are several advantages associated with this parameter. First, it is dimensionless, and thus can be scaled to the dimensions appropriate for future applications. Second, by subtracting the vertical movements of two adjacent points, one eliminates systematic errors associated with the LiDAR elevation surfaces. Finally, angular distortion is a parameter

used widely and successfully in geotechnical engineering to evaluate the effects of ground deformation on buildings (e.g., Boscardin and Cording, 1989; Clough and O'Rourke, 1990).

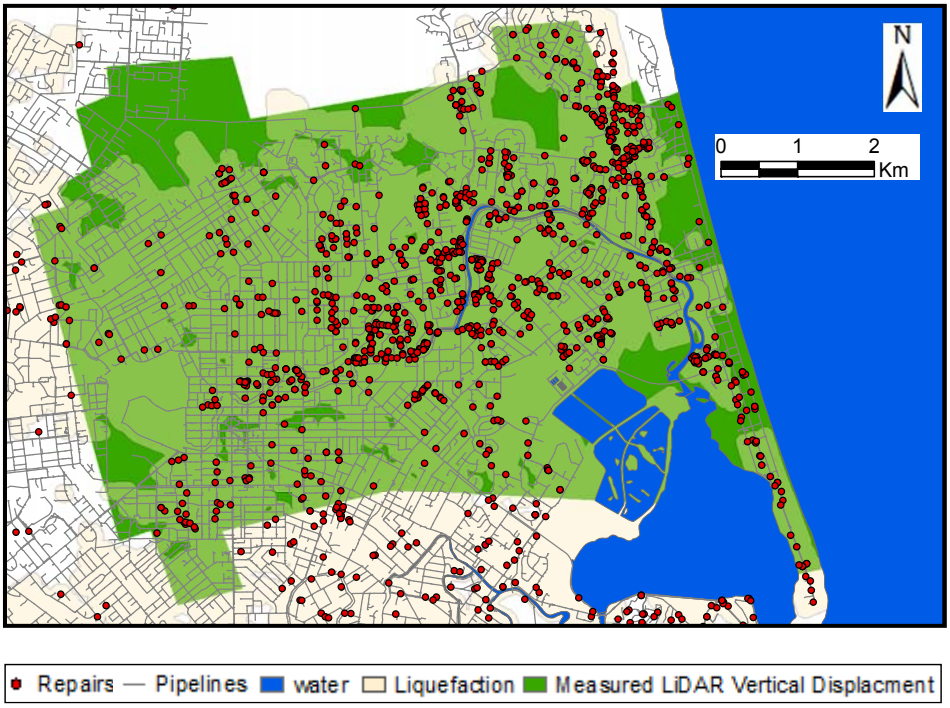

Figure 3.6. Coverage of liquefaction and measured LiDAR vertical displacement associated with pipeline distribution and repairs for 22 Feb. 2011 earthquake.

The angular distortion for each 5-m cell associated with the LiDAR measurements was calculated in the GIS analysis with a third order finite difference method proposed by Horn (1981). This method employs a third order finite difference algorithm fitted to the 8 closest vertical ground surface movement grid points in the x (E-W) and y (N-S) directions, as described by Burrough and McDonnell (1998), to calculate β at each LiDAR point.

Correlations of RR for different pipe types vs. β were developed by counting the number of repairs and pipeline lengths for the particular pipe type in each 5-m cell, and then calculating the RR associated with β intervals of 1 x 10^{-3}. The Eqn. 3.4 screening technique, with 90% confidence and α = 50%, was applied to develop the linear regressions between RR and β. The sole exception is for the correlation associated with CI pipelines, for which the confidence was relaxed a small amount to 85% so that a better dispersion of data points could be attained for the regression analysis. As a further check, the actual pipeline repairs for a particular RR were examined through GIS to screen repairs at the observed liquefaction area boundaries or associated with local concentrations of damage that were influenced by other factors. Pipelines affected by landslides and rock falls during the 22 Feb. 2011 earthquake were also screened from analysis.

As previously discussed, many wastewater pipelines damaged by the 22 Feb. 2011 earthquake had not been repaired when the 13 June 2011 earthquake occurred. To develop RR vs β regressions, the RRs were determined from the repairs recorded between 1) 23 Feb. 2011 and

the 13 June 2011 earthquake and 2) 14 June 2011 and the beginning of steady state conditions of repair. Linear regressions were then developed between the average of the two RRs associated with each β and that value of β.

The linear regressions and equations are shown in Figs. 3.7 and 3.8 for water and wastewater pipelines, respectively. Sufficient RR data for AC, CI, and PVC water pipelines that passed the screening process were available to develop the regressions in Fig. 3.7. Likewise, sufficient data for EW, RCRR, and CONC wastewater pipelines that passed the screening process were available develop the regressions in Fig. 3.8. Pipeline damage is related to the combined effects of differential vertical and lateral ground surface movement such that damage can occur in response to lateral strain when β =0, as shown in the regressions.

3.5.3 Repair Rates for Lateral Ground Surface Strain

Measurements of lateral movement derived from the LIDAR surveys are also available through CERA (2012), and are provided as displacements in the east-west (EW) and north-south (NS) directions at 56-m intervals. The horizontal spatial accuracy of the LiDAR data is between ± 400 mm and ± 500 mm (CERA, 2012). The data were corrected in this study for tectonic movements, which are also provided through CERA. For the purpose of horizontal strain calculations, the horizontal displacement data points are considered as corners of square elements shown in Fig. 3.9. The grid with square elements may be regarded as a finite element mesh with bilinear quadrilateral elements. Knowing the coordinates of each corner and the corresponding displacement, the strains in the EW and NS directions (ε_x and ε_y, respectively) and shear strains (γ_{xy}) can be calculated by computing the spatial derivatives of displacements using linear interpolation. Accordingly, finite element formulations were used to determine horizontal ground strains in the center of the elements, following the method described by Cook (1995). The strain matrix is calculated as

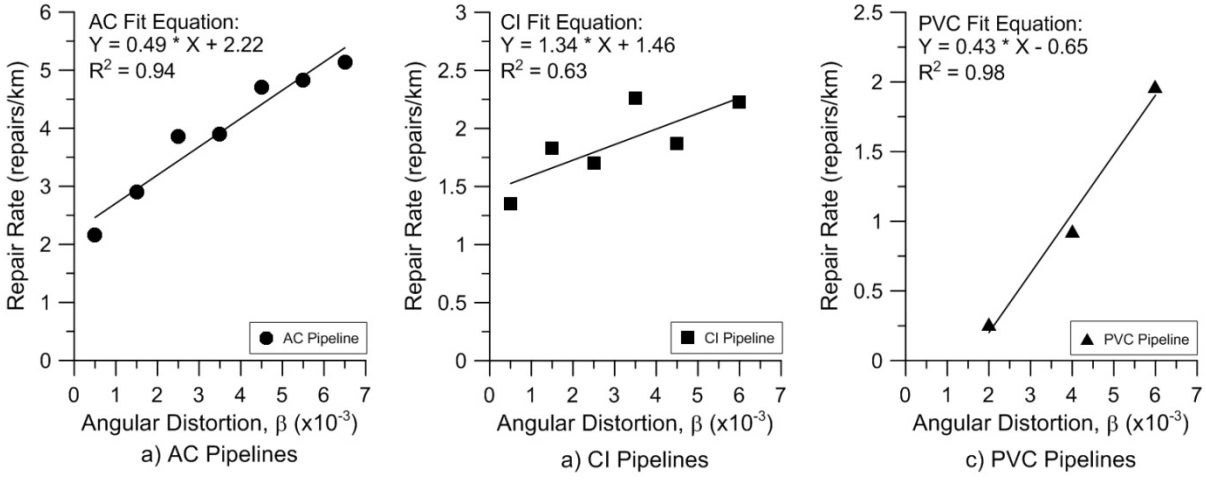

Figure 3.7. Repair rate vs. angular distortion of AC, CI, and PVC water pipelines.

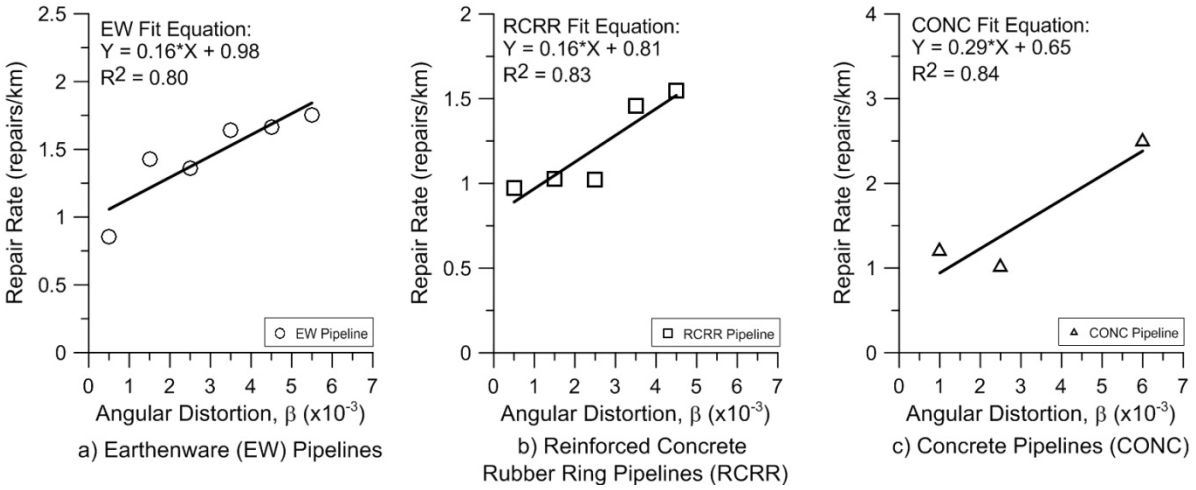

Figure 3.8. Repair rate vs. angular distortion of EW, RCRR, and CONC wastewater pipelines.

$$\begin{Bmatrix} \varepsilon_x \\ \varepsilon_y \\ \gamma_{xy} \end{Bmatrix} = \frac{1}{4a^2} \begin{bmatrix} -(a-y) & 0 & (a-y) & 0 & \cdots \\ 0 & -(a-x) & 0 & -(a+x) & \cdots \\ -(a-x) & -(a-y) & -(a+x) & (a-y) & \cdots \end{bmatrix} \begin{Bmatrix} u_1 \\ v_1 \\ u_2 \\ v_2 \\ \vdots \\ v_4 \end{Bmatrix} \tag{3.5}$$

in which u_1, v_1, u_2,...,v_4 are the corner displacements defined in Fig. 3.8, x and y are coordinates in two dimensional space, and a is the length of the square cell that is 56 m.

Using the strains from Eqn. 3.5, the principal strains, ε_1 and ε_2, were calculated from well-known strain transformations as

$$\varepsilon_{1,2} = \frac{\varepsilon_x + \varepsilon_y}{2} \pm \sqrt{\left(\frac{\varepsilon_x - \varepsilon_y}{2}\right)^2 + \left(\frac{\gamma_{xy}}{2}\right)^2} \tag{3.6}$$

Figures 3.10 and 3.11 present RR vs. lateral ground strain linear regressions for water and wastewater pipelines, respectively. The lateral ground strain is the maximum absolute value of the ground strain, ε_{HP}, given by Eqn. 3.6. The RRs were screened following procedures similar to those used with β, as previously described. Average RRs were determined following the same approach used for wastewater pipelines above to develop correlations with β.

There were sufficient RR data passing the screening criteria for AC, CI, and PVC water pipelines and EW and CONC wastewater pipelines to develop linear regressions. The regression results show a strong correlation between pipeline damage and lateral ground strains, as indicated by the relatively high r-squared values. The RRs plotted in Figs. 3.10 and 3.11 also reflect damage from differential settlement that can occur when $\varepsilon_{HP} = 0$, as shown in the regressions.

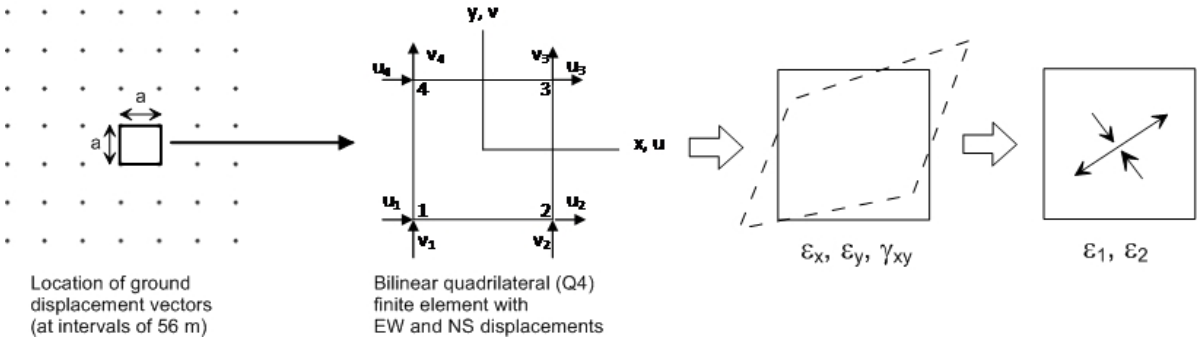

Figure 3.9. Procedure of calculating ground strains from horizontal ground displacements.

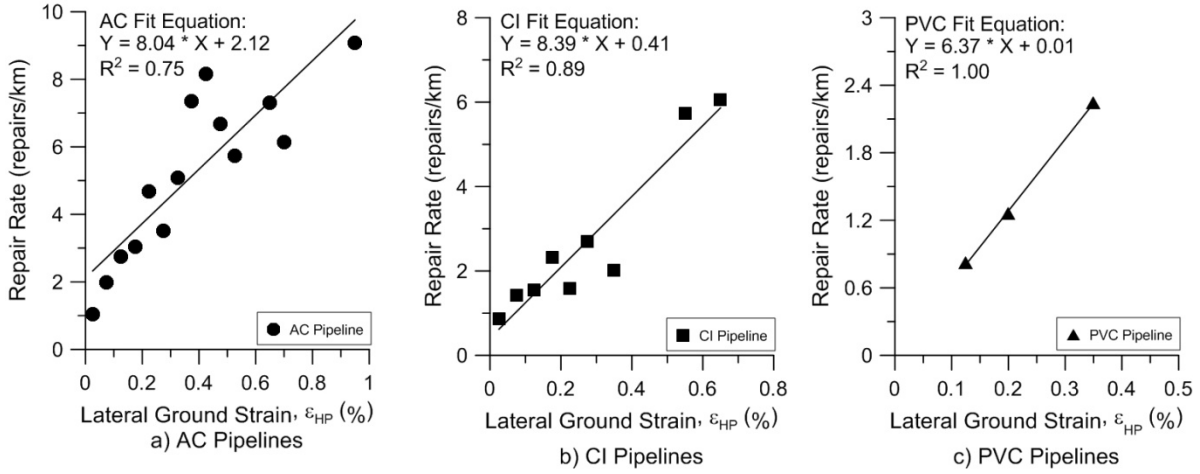

Figure 3.10. Repair rate vs. lateral ground strain correlations for AC, CI, and PVC water pipelines.

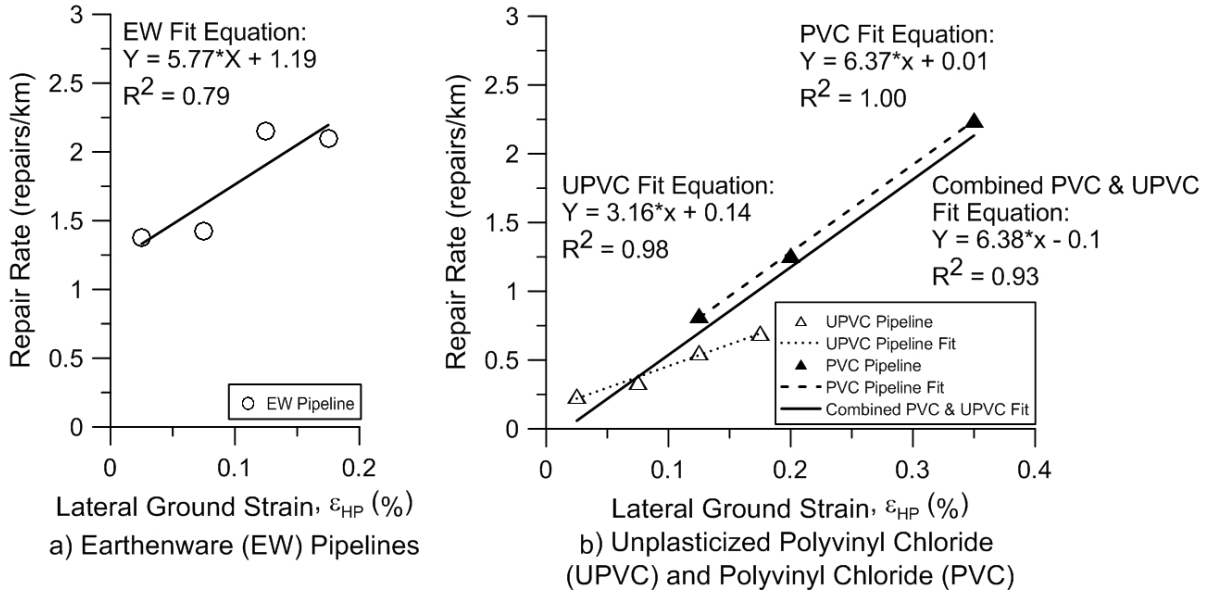

Figure 3.11. Repair rate vs. lateral ground strain correlations for EW, PVC and UPVC wastewater pipelines.

In Fig. 3.11b linear regressions for PVC, UPV and the combined data for both pipeline types are shown. Although the PVC water and UPVC wastewater pipelines differ slightly with respect to PVC additives and pipe wall thickness, they are similar with respect to strength and mechanical properties. Moreover, they are equipped with joints having similar geometries, insertion depths, and gaskets. As shown in the figure, the combined data regression provides a good fit for both data sets with high r-squared.

3.5.4 Comparison of Repair Rate Relationships

Figure 3.12a compares the regression of RR vs. β for AC, CI, and PVC water pipelines and EW, RCRR, and CONC wastewater pipelines. The figure shows that AC pipelines are especially vulnerable to differential vertical movement, with RR as much as 2 to 3 times higher than that for CI pipelines at comparable levels of β. This vulnerability is attributable in part to the use of a relatively weak AC collar to join adjacent lengths of pipe. This collar is susceptible to cracking in response to relative rotation caused by differential settlement. CI pipelines, in contrast, have additional wall thickness at the bell end of bell-and-spigot joints. Such joints are thus more resistant to stress concentrations associated with relative rotation. The fragilities of CI, EW, RCRR, and CONC pipelines are comparable, with trend lines clustered between those for AC and PVC. The PVC RRs are approximately one fourth those of the AC pipelines, representing the greatest spread in RR levels for similar β of the

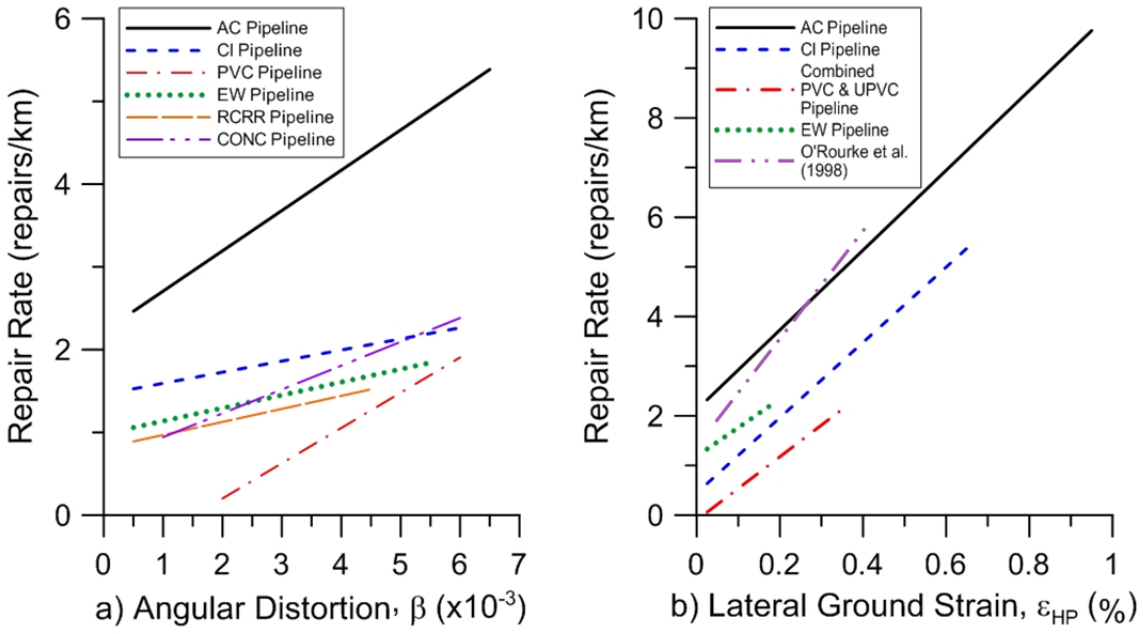

Figure 3.12. Comparison of repair rate vs. angular distortion and lateral strain for different pipe types.

pipelines under comparison. At very high levels of differential settlement the RRs for PVC pipelines converge with those of CI, EW, CONC, and RCRR pipelines.

Figure 3.12b compares the pipeline damage correlations with lateral ground strain for AC, CI, EW, PVC and UPVC pipelines. Asbestos cement pipelines have the highest RR per level of ground strain, which is approximately 3 to 5 times as high at strains exceeding 0.05 % as that for PVC pipelines. Cast iron and EW pipeline RRs plot between the trends for AC and PVC pipelines. The combined PVC and UPVC regression, as described with respect to Fig. 3.11b, is plotted in Fig. 3.12b. There is no clear convergence of damage levels for AC, EW, CI, and PVC within the range of lateral strains covered by this study.

Also shown in the figure is the linear regression reported by O`Rourke et al. (1998) for CI pipelines subject to liquefaction-induced ground deformation during the 1994 Northridge earthquake. The CI regression from the Northridge earthquake follows a trend that is consistent with the trends for AC and CI pipeline damage during the 22 Feb. 2011 earthquake. It plots higher than the Christchurch CI pipeline regression, but very close to the AC pipeline regression.

3.6 Repair Rates for Combined Effects Of Differential Vertical Ground Movement and Lateral Ground Strain

Building damage caused by ground deformation from deep excavations and tunneling is frequently evaluated for the combined effects of horizontal ground strain and angular distortion. A figure correlating the severity of building damage with respect to horizontal strain and angular distortion was developed by Boscardin and Cording (1989) from field measurements and observations at actual buildings combined with the results of analytical models of building response to ground movements. This approach is used extensively to predict and plan for the effects of ground deformation on surface structures.

In a similar manner, a damage assessment approach for AC and CI water pipelines was developed for the 22 Feb. 2011 earthquake by correlating RR with both lateral ground strain, ε_{HP}, and angular distortion, β. The correlation was performed by counting repairs and lengths of AC and CI pipelines associated with ε_{HP} and β intervals of 1×10^{-3}. Sampling for specific combinations of ε_{HP} and β results in a relatively small length for each combination. To provide a sufficient number of data points for robust interpolation, the screening criteria associated with Eqn. 3.4 were relaxed to reflect a confidence of approximately 85% and 70% for AC and CI pipelines, respectively. The corresponding RR values were plotted in a graph of ε_{HP} vs. β, and the global polynomial interpolation method in ArcGIS software was used to produce RR contours as illustrated in Fig. 3.13.

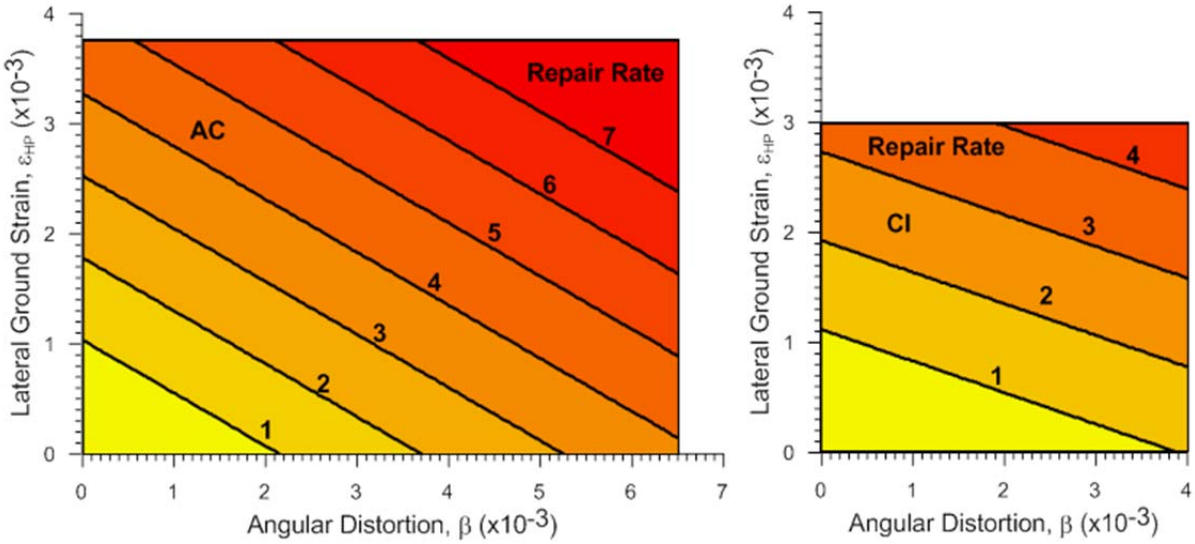

Figure 3.13. Repair rate vs lateral strain, and angular distortion for AC and CI pipelines.

As indicated in Table 3.1 there were nearly four times as many repairs for AC compared to CI pipelines in areas of observed liquefaction, thus providing a more extensive database for sampling relative to ε_{HP} and β combinations. As a result, it was possible to pass the sampling criteria for more ε_{HP} and β combinations with AC than CI pipelines, which is reflected in the relative size of the charts.

The higher vulnerability of AC pipelines is indicated by the charts, which show lower thresholds of ε_{HP} and β for a given RR compared to CI pipelines. Consistent with Figure 3.12a, AC pipelines are especially sensitive to β, with β thresholds for a given RR approximately one half those for CI pipelines.

Figure 3.13 provides the framework for predicting RR for AC and CI pipelines under the combined effects of lateral strain and differential vertical ground movement. This type of chart expands on the correlations generally used for buried pipeline fragility characterization to provide a more comprehensive treatment of ground deformation effects. Moreover, it provides a unified framework for predicting PGD effects on both buildings and underground lifelines.

3.7 Gas Distribution System Performance

Figure 3.14 shows the gas pipeline network superimposed on areas of observed soil liquefaction mapped after the 22 Feb. 2011 earthquake. As described by O'Rourke et al. (2012), the liquefied petroleum gas (LPG) system includes about 170 km of pipelines, ranging in nominal diameter from 63 mm to 315 mm; all are medium density polyethylene (MDPE) with electrofusion welds. The common pipe wall thicknesses are about 9 mm (90 mm pipe) to 14 mm (160 mm pipe). At the time of the earthquake sequence the system was about 10 to 15 years old, operating at an average network pressure of about 90 kPa.

There was virtually no damage in the pipeline network. Damage was documented in only one service line, which was tied into a concrete block subjected to ground settlement. There were two minor flange leaks on steel pipework at one of the gas terminals. There were no gas related fires.

The absence of damage is related primarily to the strength and ductility of the MDPE pipelines. High and medium density polyethylene pipelines can sustain high levels of tensile strain without rupture. When the pipelines are constructed with good workmanship using high quality electrofusion welds, there is inherent ductility in both the pipe sections and their welded connections.

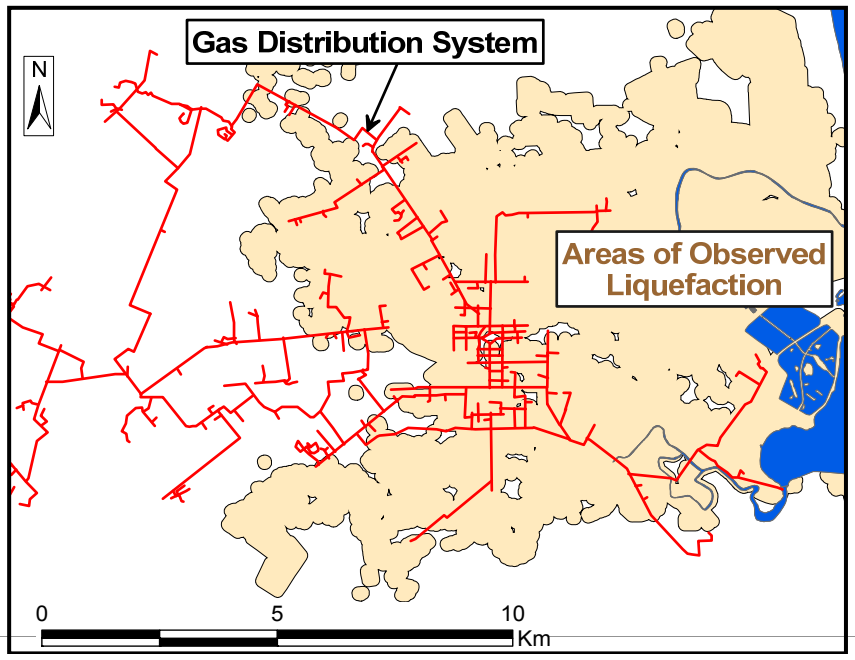

Figure 3.14. Gas distribution system and areas of observed liquefaction for the 22 Feb. 2011 earthquake.

3.8 HDPE And MDPE Pipeline Performance

After the 4 Sept. 2013 earthquake high and medium density polyethylene (HDPE and MDPE) water mains were used to replace damaged portions of the distribution system in the Burwood and Dallington areas of Christchurch. Figure 3.15 shows the location of these mains, which represent a total length of approximately 2.6 km. No damage was observed in these HDPE and MDPE pipelines after both the 22 Feb. and 13 June 2011 earthquakes, even though this area was subjected to severe liquefaction and lateral spreading of approximately 2 m after both earthquakes.

This deployment of highly ductile pipelines represents the first documented case where HDPE and MDPE pipelines were successfully installed explicitly to resist large liquefaction-induced PGD. On the basis of this experience, HDPE and MDPE mains are being used to replace damaged and vulnerable pipelines in areas vulnerable to soil liquefaction within the Christchurch distribution network, thereby improving performance in future earthquakes. The distinction between HDPE and MDPE is made on the basis of small changes in molecular weight. The yield stress and modulus of MDPE are approximately 80% of those for HDPE, and the ability to sustain bending, tension, and compression in response to ground movements are comparable for the two types of polyethylene pipelines (Stewart, et al, 2000).

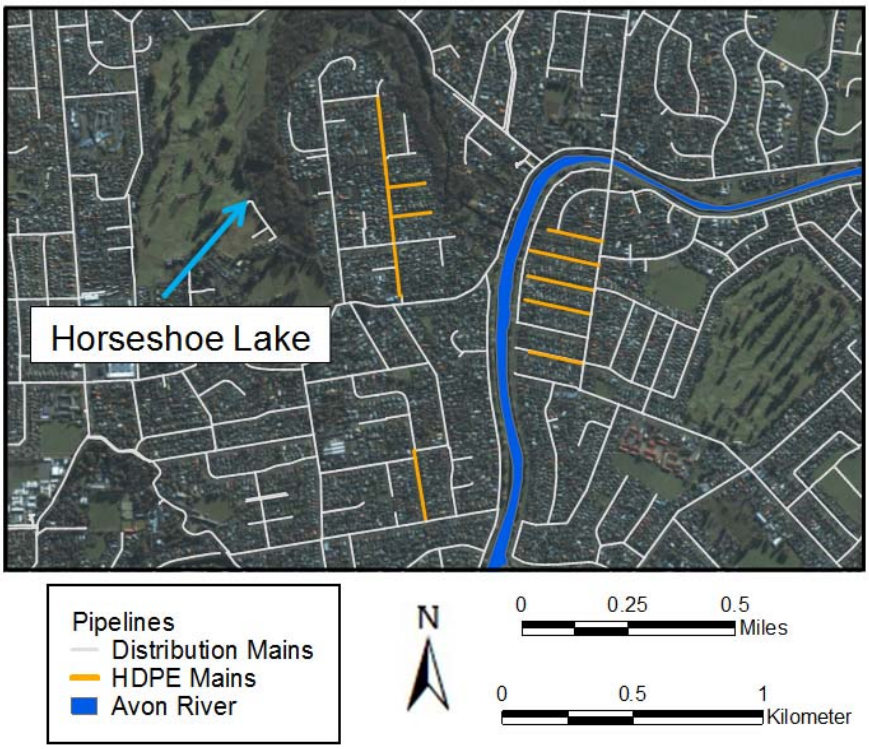

Figure 3.15. Location of HDPE pipelines installed after the Darfield earthquake.

3.9 Findings

Underground lifeline system performance during the Canterbury earthquake sequence provides a unique framework for evaluating the behavior of critical infrastructure under repeated earthquakes with substantial levels of ground motion accompanied by multiple episodes of widespread and severe liquefaction. The principal findings of the geospatial analyses are

- To select sampling lengths sufficient to produce meaningful RR statistics, screening criteria are developed, based on the assumption that pipeline repairs follow a Poisson distribution. These criteria represent an improvement over previously recommended ones, and provide a simple, robust, and flexible approach for evaluating lifeline damage caused by earthquakes.
- The Christchurch data for RR vs. GMPGV follows the trends for AC and CI pipelines observed in previous earthquakes. The inclusion of the new data provides more robust regressions for future fragility analyses of lifeline earthquake performance.
- Statistically significant regressions between RR and β and ε_{HP} are developed for AC, CI, PVC, EW, UPVC, RGRR, and CONC pipelines that can be used to predict pipeline damage in response to PGD in future earthquakes.
- The regressions quantify the relative performance of different segmental pipelines affected by liquefaction. The AC pipelines sustained damage from differential ground surface settlement at 2 to 4 times the RRs for CI, EW, CONC, and RCRR pipelines. The

AC pipelines sustained damage from lateral ground surface movement at 50 to 100% higher levels than CI and EW pipelines. The best performance with respect to differential settlement and lateral movement are shown by PVC pipelines.

- A damage assessment chart for AC and CI pipelines is developed that allows for RR prediction as a function of both ε_{HP} and β. This chart, for the first time, provides the means to estimate pipeline damage due to the combined effects of lateral and vertical ground deformation.

There were 1645 main repairs caused by the 22 Feb. 2011 earthquake, for an exceptionally high total repair rate of nearly 1 repair/km. In contrast, the Christchurch gas distribution system sustained virtually no damage in response to the combined effects of the 4 Sept. 2010, 22 Feb. 2011, 13 June 2011 and 23 Dec. 2011 earthquakes. The absence of damage is related primarily to the strength and ductility MDPE pipelines in the gas distribution system.

After the 4 Sept. 2010 earthquake HDPE and MDPE water mains were used to replace 2.6 km of the damaged distribution system. These pipelines were not damaged in response to severe liquefaction and lateral spreading as high as 2 m after the 22 Feb. and 13 June 2011 earthquakes. On the basis of this experience, HDPE and MDPE mains are being used to replace damaged and vulnerable pipelines within the Christchurch distribution network, thereby improving future earthquake performance.

The earthquake experience with HDPE pipelines in Christchurch corroborates the results of large-scale experiments at the George E. Brown, Jr. Network for Earthquake Engineering Simulation (NEES) equipment site at Cornell University (O'Rourke, et al., 2008; O'Rourke, 2010). High and medium density polyethylene pipelines can sustain high levels of tensile strain without rupture. When the pipelines are constructed with good workmanship using high quality fusion welds, there is inherent ductility in both the pipe sections and their welded connections.

4. CONCLUSIONS

The Canterbury earthquake sequence provided an exceptional opportunity to investigate the effects of varying degrees of liquefaction on critical infrastructure such as office buildings and buried utilities. Liquefaction during the earthquake sequence damaged medium and low rise reinforced concrete and steel buildings, masonry buildings, industrial facilities, and timber-frame structures, as well as lifelines, including water supply, wastewater, drainage, natural gas, electric power, telecommunications, and transportation networks. Ground deformation varied from strong shaking in the absence of permanent soil displacement to large levels of liquefaction-induced lateral spreading and settlement.

The Canterbury earthquake sequence produced varying degrees of liquefaction with differing effects on buildings, with different structural and foundation systems. In the study of structural performance in areas of the CBD, the CPT proved to be a useful site characterization tool when shallow dense gravels were not present. Its results enabled liquefaction triggering evaluations using prevalent procedures that were conservative. The conservatism in the liquefaction triggering assessments led to post-liquefaction ground settlement estimates that were generally similar for the large events in the Canterbury earthquake sequence, whereas significant building settlements and damage in the CBD were observed for the Christchurch earthquake but not for other earthquakes, such as the Darfield and June 2011 events. Moreover, the liquefaction-induced ground settlement procedures do not capture important shear-induced deformation mechanisms, such as SSI ratcheting and partial bearing failure, and the effects of ground loss due to sediment ejecta. Performance-based earthquake engineering requires improved procedures to discern between the differing levels of performance observed in Christchurch during the Canterbury earthquake sequence. Given the brittle nature of the liquefaction phenomenon as soil transforms from a stiff to a soft response rapidly as the excess pore pressure rises beyond a threshold value, the development of robust design procedures to evaluate the effects of liquefaction on buildings will be challenging. However, the case histories provided by the Canterbury earthquake sequence provide a comprehensive set of ground and building performance data for developing such methods.

Underground lifeline system performance during the Canterbury earthquake sequence also provided a unique framework for evaluating the performance of critical infrastructure under repeated earthquakes with substantial levels of ground motion accompanied by multiple episodes of widespread and severe liquefaction. Several important insights were derived from the geospatial analyses of the seismic performance of water supply, wastewater, and natural gas distribution systems during the Darfield, Christchurch, and June 2011 earthquakes. To select sampling lengths sufficient to produce meaningful RR statistics, screening criteria were developed based on the assumption that pipeline repairs follow a Poisson distribution. These criteria represent an improvement over previously recommended ones and provide a simple, robust, and flexible approach for evaluating lifeline damage caused by earthquakes. The Christchurch data for RR vs. GMPGV follows the trends for AC and CI pipelines observed in previous earthquakes. The inclusion of the new data provides more robust regressions for future fragility analyses of lifeline earthquake performance. Statistically significant regressions between RR and β and ε_{HP} were developed for AC, CI, PVC, EW, UPVC, RGRR, and CONC pipelines that can be used to predict pipeline damage in response to PGD in future earthquakes. The regressions quantify the relative performance of different segmental pipelines affected by liquefaction. The AC pipelines sustained damage from differential ground surface settlement at 2

to 4 times the RRs for CI, EW, CONC, and RCRR pipelines. The AC pipelines sustained damage from lateral ground surface movement at 50 to 100% higher levels than CI and EW pipelines. The best performance with respect to differential settlement and lateral movement are shown by PVC pipelines. Lastly, a damage assessment chart for AC and CI pipelines was developed that allows for RR prediction as a function of both ε_{HP} and β. This chart provides the means to estimate pipeline damage due to the combined effects of lateral and vertical ground deformation.

There were 1645 main repairs caused by the Christchruch earthquake, which resulted in an exceptionally high total repair rate of nearly 1 repair/km. In contrast, the Christchurch gas distribution system sustained virtually no damage in response to the effects of the Canterbury earthquake sequence. The absence of damage is related primarily to the strength and ductility MDPE pipelines in the gas distribution system. After the Darfield earthquake, HDPE and MDPE water mains were used to replace 2.6 km of the damaged distribution system. These pipelines were not damaged in response to severe liquefaction and lateral spreading as high as 2 m after the Christchurch and June 2011 earthquakes. On the basis of this experience, HDPE and MDPE mains are being used to replace damaged and vulnerable pipelines within the Christchurch distribution network, thereby improving future earthquake performance. High and medium density polyethylene pipelines can sustain high levels of tensile strain without rupture. When the pipelines are constructed with good workmanship using high quality fusion welds, there is inherent ductility in both the pipe sections and their welded connections.

Research on the effects of the Canterbury earthquake sequence provides an unprecedented opportunity to develop an integrated understanding of how critical infrastructure performs in a major earthquake with extensive and damaging liquefaction. Rarely has detailed information about lifeline and building performance been available to the degree that exists for Christchurch where the liquefaction effects of several earthquakes can be documented in a comprehensive way for both buildings and lifelines. It is hoped that these investigations will provide the underlying data and understanding for advancing an integrated examination of the impacts of liquefaction on critical infrastructure in the United States.

5. ACKNOWLEDGMENTS

This research was supported by the United States Geological Survey (U.S.G.S.), Department of the Interior, under U.S.G.S. award number G12AP20034. We gratefully acknowledge the financial support provided by the U.S.G.S. for this work. This project was part of a larger collaborative research project that included other sponsors in addition to the U.S.G.S. The primary support for the NZ researchers was provided by the Earthquake Commission New Zealand (EQC) and the University of Canterbury. Support for the US researchers was provided by the U.S.G.S. award number G12AP20034, and grants from the U.S. National Science Foundation (NSF) through CMMI-0825734 and CMMI-1137977. This work also incorporates research results supported by the George E. Brown, Jr. Network for Earthquake Engineering Simulation (NEES) Program of NSF under Grant No. CMMI-1041498. The views and conclusions contained in this document are those of the authors and should not be interpreted as necessarily representing the official policies, either expressed or implied, of the U.S. Government, the EQC, or the NSF.

We would also like to acknowledge the assistance of all NZ and US GEER team members who participated in the reconnaissance of these events. Their contributions are noted at: http://www.geerassociation.org/. Thanks are extended to the Christchurch Earthquake Recovery Authority (CERA), Stronger Christchurch Infrastructure Rebuild Team (SCIRT), Christchurch City Council (CCC), Earthquake Commission (EQC), Contact Energy, and Tonkin and Taylor Ltd for their assistance. All LiDAR survey and liquefaction observation data are available through the CERA (2012) and were provided courtesy of EQC. In addition, special thanks are extended to Professor Russell Green, Professor Brady Cox, Dr. Brendon Bradley, Kelly Robinson, Simona Giorgini, Ian McCahon, Mike Jacka, Iain Haycock, Richard Wise, and Nathan Barnes, Hugh Cowan of EQC, John Noonan of SCIRT, and Rowan Smith and Wai Yu of Contact Energy.

6. REFERENCES

Bardet, J.P., Ballantyne, D., Bell, G.E.C., Donnellan, A., Foster, S., Fu, T., List, J., Little, R.G., O'Rourke, T.D., and Palmer, M.C. (2010) Expert Review of Water System Pipeline Breaks in the City of Los Angeles during Summer 2009, *Report to the Steering Committee on Water Pipeline Breaks of the City of Los Angeles*, Los Angeles, CA, April.

Beca (2011) Verticality Survey. *Geotechnical Report*, April.

Boscardin, M.D., and Cording, E.J. (1989) Building response to excavation-induced settlement. *Journal of Geotechnical Engineering*, ASCE **115(1)**, 1-21.

Bradley, B.A., (2010) NZ-specific pseudo-spectral acceleration ground motion prediction equations based on foreign models. *Department of Civil and Natural Resources Engineering, University of Canterbury,* Christchurch, New Zealand. 324 pp.

Bradley, B.A., Hughes, M., (2012) Conditional Peak Ground Accelerations in the Canterbury Earthquakes for Conventional Liquefaction Assessment. *Technical Report Prepared for the Department of Building and Housing,* 22 pp.

Bray, J.D., and Dashti, S. (2010) Liquefaction-Induced Movements of Buildings with Shallow Foundations. *Fifth Inter. Conf. on Rec. Adv. in Geo. EQ Engrg. & Soil Dyn*., May 24-29, San Diego, CA, Paper No. OSP-2.

Brown, L.J., and Weeber, J.H., (1992) Geology of the Christchurch urban area. *New Zealand, Institute of Geological and Nuclear Sciences*, Lower Hutt, 1992.

Brown, L.J., Beetham, R.D., Paterson, B.R., Weeber, J.H. (1995) Geology of Christchurch, New Zealand.*Environmental and Engineering Geosciences,* Vol. 1, No. 4, pp. 427-488.

Burrough P.A., and McDonnell, R.A. (1998) Principles of Geographical Information Systems, *Oxford University Press*, Oxford, U.K.

Canterbury Earthquake Recovery Authority (CERA) (2012) Geotechnical database for Canterbury earthquake sequence, NZ. at (accessed August 2012): https://canterburygeotechnicaldatabase.projectorbit.com.

Canterbury Geotechnical Database (2012) Aerial Photography. Map Layer CGD0100 - 1 June 2012, retrieved 20 Dec. 2012 from: https://canterburygeotechnicaldatabase.projectorbit.com/ Liquefaction Interpreted from Aerial Photography. Map Layer CGD0200 - 23 July 2012, retrieved 20 December, 2012 from: https://canterburygeotechnicaldatabase.projectorbit.com/ Vertical Ground Surface Movements. Map Layer CGD0600 - 23 July 2012, retrieved 13 January 2013 from: https://canterburygeotechnicaldatabase.projectorbit.com/

Christchurch City Council (2006) Water Supply Asset Management Plan, Section 2. Christchurch City Council, Christchurch, NZ, September.

Clough, G.W., and O'Rourke, T.D. (1990) Construction induced movements of in-situ walls, in *Proceedings, Specialty Conference on Design and Performance of Earth Retaining Structures*, ASCE, 439-470.

Cook, R. D. (1995). *Finite Element Modeling For Stress Analysis*, NY, John Wiley and Sons.

Cubrinovski, M., Bray, J.D., Taylor, M., Giorgini, S., Bradley B.A., Wotherspoon, L., and Zupan, J. (2011a) Soil liquefaction effects in the central business district during the February 2011 Christchurch earthquake, *Seismological Research Letters,* **82,** 893-904.

Cubrinovski, M., Bradley, B., Wotherspoon, L., Green, R., Bray, J., Wood, C., Pender, M., Allen, J., Bradshaw, A., Rix, G., Taylor, M., Robinson, K., Henderson, D., Giorgini, S., Ma, K., Winkley, A., Zupan, J., O'Rourke, T., DePascale, G. and Wells, D. (2011b) Geotechnical

Aspects of the 22 February 2011 Christchurch earthquake. *Bulletin of the New Zealand Society of Earthquake Engineering* 44(4): 205-226.

Cubrinovski, M., Green, R.A., and Wotherspoon, L. [Eds] (2011c) Geotechnical Reconnaissance of the 2011 Christchurch Earthquake. *Technical Report,* retrieved from: http://geerassociation.org/GEER_Post%20EQ%20Reports/Christchurch_2011/Index_Christchurch_2011.html.

Eliot Sinclair and Partners Ltd. (2011) Ground Floor Levels 4/3/11. March.

Geonet (2011) Processed Strong Ground Motions. available at ftp://ftp.geonet.org.nz/strong/processed/Proc/2011/ (accessed August 2012).

GNS Science (2011) The Canterbury earthquake sequence and implications for seismic design levels, *GNS Science Consultancy Report 2011/183*, commissioned by the Canterbury Earthquakes Royal Commission, NZ, October.

GNS Science (2013) The most recent aftershock map. available at: http://www.gns.cri.nz/Home/Our-Science/Natural-Hazards/Recent-Events/Canterbury-quake/Recent-aftershock-map (accessed February 2013).

Green, R.A., and Cubrinovski, M. [Eds] (2010) Geotechnical Reconnaissance of the 2010 Darfield (New Zealand) Earthquake.*TechnicalReport.*Retrieved from: http://www.geerassociation.org/GEER_Post%20EQ%20Reports/Darfield%20New%20Zealand_2010/Darfield_New%20Zealand_2010_index.html

Horn, B.K.P. (1981) Hill shading and the reflectance map, *Proceedings, IEEE* **69(1)**, 14-47.

Idriss, I.M, and Boulanger, R.S (2008) Soil Liquefaction During Earthquakes. *Earthquake Engineering Research Institute*, EERI MNO-12, Oakland, CA.

Ishihara, K., and Yoshimine, M. (1992) Evaluation of settlements in sand deposits following liquefaction during earthquakes. *J. Soils and Foundations*, 32(1), 173-188.

Jeon, S.-S. (2002) Earthquake performance of pipelines and residential buildings and rehabilitation with cast-in-place pipe lining systems, *Ph.D. Thesis, Cornell University*, Ithaca, NY.

Jeon, S.-S., and O'Rourke, T.D. (2005) Northridge earthquake effects on pipelines and residential buildings, *Bulletin of the Seismological Society of America* **95-1**, 1-25.

Moss, R.E.S., Seed, R.B., Kayen, R.E., Stewart, J.P., Der Kiureghian, A., and Cetin, K.O. (2006) CPT-Based Probabilistic and Deterministic Assessment of In Situ Seismic Soil Liquefaction Potential. *J. Geotech. Geoenviron. Eng.*, 132(8), 1032-1051

O'Rourke, M.J, and Deyoe, E. (2004) Seismic damage to segmented buried pipe, *Earthquake Spectra* **20**, 1167–1183.

O'Rourke, M.J., and Liu, X. (1999) Response of Buried Pipelines Subject to Earthquake Effects. *Monograph No. 3, Multidisciplinary Center for Earthquake Engineering Research*, Buffalo, NY.

O'Rourke, T.D. (2010) Geohazards and large geographically distributed systems, *Geotechnique* **50(7)**, 503-543.

O'Rourke, T. D., Toprak, S., and Sano, Y. (1998) Factors Affecting Water Supply Damage Caused by the Northridge Earthquake, *Proceedings, 6th US National Conference on Earthquake Engineering*, Seattle, WA, 1-12.

O'Rourke, T. D., Jeon, S.-S., Toprak, S., Cubrinovski, M., and Jung, J.K. (2012) Underground Lifeline System Performance during the Canterbury Earthquake Sequence, *Proceedings, 15th World Conference in Earthquake Engineering,* Lisbon, Portugal, September.

O'Rourke, T.D., Jezerski, N.A., Olson, T., Bonneau, A.L., Palmer, M.C., Stewart, H.E., O'Rourke, M. J., and Abdoun, T. (2008) Geotechnics of Pipeline System Response to Earthquakes*, Proceedings, Geotechnical Earthquake Engineering and Soil Dynamics IV (GEESD)*, Sacramento, CA, May.

Robertson, P.K., and Wride, C.E. (1998) Evaluating cyclic liquefaction potential using the cone penetration test. *Can. Geotech. J.,* 35, 442-459.

Ruamoko Solutions (2010) Earthquake Damage Inspection Report. report prepared for Shipleys Audiovisual Ltd., Dec.

Soils and Foundations (1987) Site Investigation Report. report prepared for Tyndall and Hanham Consulting Engineers, Feb.

Stewart, H.E., Bilgin, O., O'Rourke, T.D., and Keeney, T. (2000) Improved Design and Construction Practices for Thermal Loads in Plastic Gas Pipelines, *Final Report GRE Contract No. 5095-207-2821*, Gas Research Institute, Chicago.

Taylor M.L., Cubrinovski, M., and Bradley, B.A. (2012) Characterisation of Ground Conditions in the Christchurch Central Business District," *Australian Geomechanics Journal*, Vol. 47(4), pp. 43-57.

Tonkin and Taylor (2011) Christchurch Central City Geological Interpretive Report. report prepared for the Christchurch City Council, Dec. (Ver. 1.1).

Tonkin and Taylor (2012) Groundwater Depth Maps. preliminary data shared by T&T.

Trautmann, C.H., O'Rourke, T.D., Grigoriu, M.D., and Khater, M.M. (1986) Systems Model for Water Supply Following Earthquakes, *Lifeline Seismic Risk Analysis - Case Studies*, Eguchi, R. Ed., ASCE, 30-50.

Zhang, G., Robertson, P.K., and Brachman, R.W.I. (2002) Estimating liquefaction-induced ground settlements from CPT for level ground. *Can. Geotech. J.,* 39, 1168-1180.

BIBLIOGRAPHY

Bray, J.D., Cubrinovski, M., Zupan, J., and Taylor, M. (2013). "Liquefaction Effects on Buildings in the Central Business District of Christchurch," *Earthquake Spectra,* under review.

O'Rourke, T. D., Jeon, S.-S., Toprak, S., Cubrinovski, M., and Jung, J.K. (2012). "Underground Lifeline System Performance during the Canterbury Earthquake Sequence"*, Proceedings, 15th World Conference in Earthquake Engineering,* Lisbon, Portugal, September.

O'Rourke, T.D., Jeon, S., Toprak, S., Cubrinovski, M., Hughes, M., van Ballegooy, S., and Bouziou, D. (2013). "Earthquake Performance of Underground Lifelines in Christchurch, NZ," *Earthquake Spectra,* under review.